



CERN-EP-2022-076
30 March 2022

W[±]-boson production in p–Pb collisions at $\sqrt{s_{NN}} = 8.16$ TeV and Pb–Pb collisions at $\sqrt{s_{NN}} = 5.02$ TeV

ALICE Collaboration*

Abstract

The production of the W[±] bosons measured in p–Pb collisions at a centre-of-mass energy per nucleon–nucleon collision $\sqrt{s_{NN}} = 8.16$ TeV and Pb–Pb collisions at $\sqrt{s_{NN}} = 5.02$ TeV with ALICE at the LHC is presented. The W[±] bosons are measured via their muonic decay channel, with the muon reconstructed in the pseudorapidity region $-4 < \eta_{lab}^{\mu} < -2.5$ with transverse momentum $p_{T}^{\mu} > 10$ GeV/c. While in Pb–Pb collisions the measurements are performed in the forward ($2.5 < y_{cms}^{\mu} < 4$) rapidity region, in p–Pb collisions, where the centre-of-mass frame is boosted with respect to the laboratory frame, the measurements are performed in the backward ($-4.46 < y_{cms}^{\mu} < -2.96$) and forward ($2.03 < y_{cms}^{\mu} < 3.53$) rapidity regions. The W⁻ and W⁺ production cross sections, lepton-charge asymmetry, and nuclear modification factors are evaluated as a function of the muon rapidity. In order to study the production as a function of the p–Pb collision centrality, the production cross sections of the W⁻ and W⁺ bosons are combined and normalised to the average number of binary nucleon–nucleon collision $\langle N_{coll} \rangle$. In Pb–Pb collisions, the same measurements are presented as a function of the collision centrality. Study of the binary scaling of the W[±]-boson cross sections in p–Pb and Pb–Pb collisions is also reported. The results are compared with perturbative QCD calculations, with and without nuclear modifications of the Parton Distribution Functions (PDFs), as well as with available data at the LHC. Significant deviations from the theory expectations are found in the two collision systems, indicating that the measurements can provide additional constraints for the determination of nuclear PDFs and in particular of the light-quark distributions.

© 2022 CERN for the benefit of the ALICE Collaboration.

Reproduction of this article or parts of it is allowed as specified in the CC-BY-4.0 license.

*See Appendix A for the list of collaboration members

1 Introduction

The production of the W[±]- and Z⁰-vector bosons is extensively studied at hadron colliders. The W[±] and Z⁰ bosons are weakly interacting particles, produced early in hadronic collisions (with a formation time $t_f \sim 1/M \sim 10^{-3}$ fm/c), predominantly via the Drell-Yan process in which a quark–antiquark pair annihilates into a lepton pair [1, 2]. Due to their large masses, $M_{W^\pm} = 80.379 \pm 0.012$ GeV/c² and $M_{Z^0} = 91.1876 \pm 0.0021$ GeV/c² [3], their production is well described within the perturbative quantum chromodynamics (pQCD) framework, up to Next-to-Next-to-Leading Order (NNLO) by means of the QCD factorisation theorem for hard processes [4, 5]. Factorisation allows us to separate the short distance part of the cross section, corresponding to the partonic cross section that can be expanded perturbatively, from the long distance part containing the Parton Distribution Functions (PDFs), parameterising the partonic content of the nucleon and determined from experimental data. The input parameters for theoretical calculations, such as the boson masses or the weak couplings, are known with high accuracy, enabling the usage of measurements of the electroweak-boson production to determine the up (u), down (d) and to a lesser extent strange (s) PDFs (see Refs. [6, 7] for recent reviews). In nuclear collisions, the presence of a nuclear environment affects the inner structure of the nucleon, requiring the determination of nuclear PDFs (nPDFs). As for the free-nucleon case, the nPDFs are obtained from a global analysis of the available data, but in this case the results are mostly constrained by Deep-Inelastic Scatterings (DIS) and Drell-Yan data in a limited region of the four-momentum transfer squared Q^2 and parton longitudinal momentum fraction x (Bjorken- x). The resulting nPDF uncertainties drastically limit the precision of theoretical calculations and their ability to describe and predict processes in nuclear collisions. In order to further constrain the nPDFs and reduce their uncertainties, the production of the W[±] and Z⁰ bosons has been measured in proton–lead (p–Pb) and lead–lead (Pb–Pb) collisions at the CERN Large Hadron Collider (LHC) by the four main experiments, at midrapidity by ATLAS and CMS [8–19] and at large rapidities by ALICE and LHCb [20–23].

Four main intervals of Bjorken- x featuring different nuclear modifications can be distinguished at high Q^2 values. The nPDFs show a suppression at low Bjorken- x , for $x \lesssim 0.05$, and an enhancement within the range $x \sim 0.05 - 0.3$ ¹. Both these effects, referred to as shadowing and anti-shadowing, respectively, originate from destructive or constructive interferences of amplitudes arising from multiple scatterings between partons in the nucleus [24]. Another depletion region is seen for x within 0.3 – 0.9 in the so-called EMC-effect region which is not yet fully understood [25]. Finally, for x larger than 0.9 the Fermi motion of the nucleons inside the nucleus yields an enhancement of the PDF [26]. These effects will naturally affect the production of electroweak bosons [27], and their measurement provides a unique opportunity to constrain the nPDFs at high $Q^2 \sim M_{W,Z}^2$. Moreover, with the large luminosities and centre-of-mass energies delivered by the LHC, combined with the wide acceptance covered by the LHC experiments, the study of electroweak bosons has become accessible in p–Pb and Pb–Pb collisions over a large Bjorken- x range, from almost unity down to $x \sim 10^{-4}$ where the experimental constraints are scarce. Measurements in p–Pb collisions at large negative and positive rapidities are of high interest as they allow the disentanglement of the high ($\sim 10^{-1}$) and low ($\sim 10^{-4} - 10^{-3}$) Bjorken- x intervals, respectively. The yields of the W[−] and W⁺ bosons, mainly produced by interactions between u and d quarks via the $d\bar{u} \rightarrow W^-$ and $u\bar{d} \rightarrow W^+$ processes, offer a probe of the light quark PDFs, while their asymmetry is sensitive to the down-to-up ratio in the nucleus [28]. The leptonic decay of these bosons is of particular interest, as the decay products do not interact strongly, therefore being blind to the quark–gluon plasma (QGP), the hot and dense medium created in heavy-ion collisions. In addition, the in-medium energy loss of the decay leptons by bremsstrahlung is negligible [29]. Combined with the colourless nature of the W[±] boson itself, this physics channel provides a medium-blind process and consequently, a direct probe of the initial state of the collision even in the presence of a QGP. The production of electroweak bosons, therefore, enables the study of the nPDFs of the colliding nuclei.

¹All the Bjorken- x ranges are indicative, as the precise values of the region boundaries depend on the parton flavour, the nPDF parametrisation, and the Q^2 scale.

The measurements of the W[±]-boson production presented in this publication are compared with predictions obtained from calculations at Next-to-Leading Order (NLO), implementing the nuclear modifications of the PDFs using the EPPS16 [30], nCTEQ15 [31] and nNNPDF2.0 [32] sets, in which the parametrisation and determination of the nPDF follow different approaches. The approach of the EPPS (formerly EPS) group introduces, for a given parton i in a nucleus with atomic number A , the nuclear correction factor $R_i(x, A)$ at the input parametrisation scale Q_0^2 . In such a model, the nPDF set is composed of nuclear modification functions to be applied to a free-nucleon PDF set which serves as a baseline. The approach of the nCTEQ collaboration does not utilise the nuclear correction factors, instead, it is a full nPDF parametrisation. It starts from the functional form used for the free-proton PDF (in the nCTEQ case the form is similar to the CTEQ6 parametrisation [33]), with the addition of A -dependent free parameters. The lack of experimental data that can be used for the nPDF determination induces a strong dependence of the models on the phenomenological and methodological assumptions. The EPPS16 and nCTEQ15 sets show large differences in the predicted nuclear modifications and associated uncertainties [34], originating from the functional form, the number of free parameters, and the data points included in the global analysis. In order to reduce the parametrisation bias, the nNNPDF collaboration adopted the methodology described in Ref. [35], and used artificial neural networks as universal, unbiased interpolants to parametrise the x and A dependence of the nPDFs. Recently, the LHC experiments contributed to the evolution of the models, and W[±] and Z⁰ measurements in p–Pb collisions are now included into the input datasets, in EPPS starting with EPPS16 [30], in nCTEQ after the nCTEQ15WZ update [36], and in nNNPDF from their 2.0 release [32]. It should be noted that the EPPS model has recently been updated with the release of the EPPS21 set [37]. The production of electroweak bosons calculated from this set is in fair agreement with the ones obtained with the EPPS16 model, with a significant reduction of the associated uncertainties.

In this article, the ALICE results on the measurement of the W[±]-boson production via the muonic decay channel in p–Pb collisions at a centre-of-mass energy per nucleon–nucleon collision $\sqrt{s_{\text{NN}}} = 8.16$ TeV and Pb–Pb collisions at $\sqrt{s_{\text{NN}}} = 5.02$ TeV are reported. These results constitute the first measurements of the W[±]-boson production at large rapidities for these collision systems and energies, with the p–Pb results complementing the CMS measurements at midrapidity [15] and extending the ALICE measurements in p–Pb collisions at $\sqrt{s_{\text{NN}}} = 5.02$ TeV [20]. The paper is structured as discussed in the following. Section 2 introduces the ALICE apparatus, focusing on the detectors relevant for the analyses, followed by a description of the event and track selections. The analysis strategy, including the procedure for the signal extraction and the simulation of the apparatus, is presented in Section 3, together with a discussion of the systematic uncertainties. The results are reported in Section 4 where they are compared with theoretical predictions and other published measurements. A summary of the results and their interpretation is given in Section 5.

2 ALICE apparatus and data samples

2.1 The ALICE detector

The W[±] bosons are detected through their muonic decay channel via the $W^- \rightarrow \mu^- \bar{\nu}_\mu$ process and its charge conjugate, with a branching ratio $\text{BR} = (10.63 \pm 0.15)\%$ [3], from data recorded with the ALICE muon spectrometer [38, 39]. The spectrometer covers in full azimuth the $-4 < \eta_{\text{lab}} < -2.5$ pseudorapidity interval². Its tracking system is composed of five stations, each made of two planes of cathode pad chambers. The third station sits inside a dipole magnet providing an invertible magnetic field with integrated intensity of 3 Tm, which bends the trajectory of charged particles thus enabling the measurement of the track momentum. The muon system also includes a muon trigger, consisting

²In the ALICE reference frame, the muon spectrometer covers negative η . In symmetric collisions such as Pb–Pb, positive values of rapidity are conventionally used for the muon coverage. In p–Pb collisions, by convention, the proton beam moves towards positive rapidities.

of four planes of resistive plate chambers arranged in two stations. The whole spectrometer is shielded by a set of absorbers. A conical absorber of 10 interaction lengths (λ_i) made of carbon, concrete, and steel is located in front of the muon spectrometer, filtering out hadrons and low-momentum muons from the decays of light particles such as pions and kaons. The trigger stations are located behind a 1.2 m thick (about $7.2 \lambda_i$) iron wall, absorbing hadrons punching through the front absorber as well as low-momentum secondary muons. Finally, a high-density cylinder made of tungsten and lead, the so-called small-angle absorber, surrounds the beam pipe throughout the muon spectrometer in its entirety and shields it against secondary particles produced by the interaction of primary particles at large η with the beam pipe.

Other detectors are needed for primary vertex reconstruction, triggering on Minimum Bias (MB) collisions, multiplicity determination, and centrality evaluation. The primary interaction vertex reconstruction is performed using the Silicon Pixel Detector (SPD), the two innermost layers of the Inner Tracking System (ITS) [40], covering the pseudorapidity intervals $|\eta_{\text{lab}}| < 2.0$ and $|\eta_{\text{lab}}| < 1.4$. The V0 detector [41] is made of two arrays of scintillator tiles, located asymmetrically around the collision point, along the beam direction, at $z = 3.4$ m (V0A) and $z = -0.9$ m (V0C), and covering the pseudorapidity intervals $2.8 < \eta_{\text{lab}} < 5.1$ and $-3.7 < \eta_{\text{lab}} < -1.7$, respectively. The V0 provides an online MB trigger through the logical coincidence of a signal in the two arrays, and participates in the determination of the luminosity by providing a reference process for van der Meer scans [42]. It is also used for the evaluation of the centrality in Pb–Pb collisions by means of a Glauber model fit [43, 44] to the sum of the signal amplitudes in the two arrays (the V0M estimator). This allows one to classify the events in centrality classes corresponding to a percentile of the total hadronic cross section. The centrality evaluated in this way relies on the event charged-particle multiplicity, a method which has been shown to be strongly biased in p–Pb collisions [45]. Instead, the centrality estimation for this system uses the Zero Degree Calorimeter (ZDC) [46], a set of two hadronic calorimeters located along the beam pipe, on both sides of the collision point, 112.5 m away from it. The timing information delivered by the V0 and ZDC detectors also helps to reduce the beam-induced background. A complete description of the ALICE detector can be found in Ref. [47] and its performance is reported in Ref. [48], where standard detection, reconstruction, and analysis procedures are described.

2.2 Event and track selections

The analysis in p–Pb collisions uses the data samples collected in 2016 at $\sqrt{s_{\text{NN}}} = 8.16$ TeV. These data were taken in two colliding beam configurations, with either the protons or lead ions moving towards the spectrometer, hereafter referred to as the p-going and Pb-going configurations, respectively. By convention, the protons move towards positive rapidities. Because of the single magnet design of the LHC, the proton and Pb beams have the same magnetic rigidity, leading to different energies per nucleon, amounting to 6.5 TeV for the protons and 2.56 TeV for the Pb ions. The resulting nucleon–nucleon centre-of-mass system is thus boosted with respect to the laboratory frame, resulting in a rapidity shift of $\Delta y_{\text{cms/lab}} = 0.465$ in the direction of the proton beam. The rapidity acceptance of the spectrometer in the centre-of-mass system is then $2.03 < y_{\text{cms}} < 3.53$ in the p-going direction and $-4.46 < y_{\text{cms}} < -2.96$ in the Pb-going one. The analysis in Pb–Pb collisions uses the data samples collected in 2015 and 2018 at $\sqrt{s_{\text{NN}}} = 5.02$ TeV in the rapidity range $2.5 < y_{\text{cms}}^\mu < 4$. For each sample, two sub-periods can be distinguished according to the sign of the magnetic field delivered by the dipole magnet.

The analysed data samples consist of events with at least one muon track candidate selected by the muon trigger system, with an online selection on the transverse momentum (p_{T}^μ) requiring it to be above $\simeq 4.2$ GeV/ c (at the threshold, the track produces a trigger signal with a 50% probability), in coincidence with a MB signal in the V0 detector. The Pb–Pb analysis is limited to the most central 90% of the total hadronic cross section, where the MB trigger is fully efficient and electromagnetic interactions are negligible. The events were further required to have a reconstructed vertex position along the beam direction within ± 10 cm from the nominal interaction point in order to keep the full efficiency of the SPD

Table 1: Average number of binary nucleon–nucleon collisions $\langle N_{\text{coll}}^{\text{mult}} \rangle$ estimated with the hybrid method for the ZN centrality classes in p–Pb collisions at $\sqrt{s_{\text{NN}}} = 8.16$ TeV [52].

Centrality class	0–100%	0–20%	20–40%	40–60%	60–100%
$\langle N_{\text{coll}}^{\text{mult}} \rangle$	7.09 ± 0.28	12.2 ± 0.52	9.81 ± 0.17	7.09 ± 0.29	3.17 ± 0.09

Table 2: Average nuclear overlap function $\langle T_{\text{AA}} \rangle$ evaluated with a Glauber MC fit to the sum of the V0 amplitudes in Pb–Pb collisions at $\sqrt{s_{\text{NN}}} = 5.02$ TeV [52].

Centrality class	0–90%	0–10%	10–20%	20–40%	40–90%
$\langle T_{\text{AA}} \rangle$ (mb ⁻¹)	6.28 ± 0.06	23.26 ± 0.17	14.40 ± 0.13	6.93 ± 0.09	1.00 ± 0.02

for vertex reconstruction. Events in which two or more interactions occur in the same colliding bunch (in-bunch pile-up) or during the readout time of the SPD (out-of-bunch pile-up), amounting to about 20% of the sample, are removed using the information from the SPD and V0 detectors. The integrated luminosity was evaluated by estimating the equivalent number of MB events corresponding to the muon-triggered data sample and then dividing by σ_{V0M} , the V0 visible cross section measured by means of van der Meer scans [42, 49, 50]. The number of MB events corresponding to the muon-triggered sample was evaluated as $N_{\text{MB}} = F_{\mu\text{-trig}/\text{MB}} \times N_{\mu\text{-trig}}$, where $N_{\mu\text{-trig}}$ is the number of muon-triggered events and $F_{\mu\text{-trig}/\text{MB}}$ is the inverse of the probability to have a muon trigger in a MB event. The value of the normalisation factor $F_{\mu\text{-trig}/\text{MB}}$ was evaluated with two different methods, either by applying the muon trigger condition in the analysis of MB events, or by comparing the counting rate of the two triggers, both corrected for pile-up effects. The nominal value was obtained from the method using the trigger rates, while the difference between the two methods was taken as the systematic uncertainty on the normalisation factor. This uncertainty amounts to 1.4% (1.1%) in p–Pb collisions for the p-going (Pb-going) configuration, and to 1% in Pb–Pb collisions. The integrated luminosities of the considered p–Pb data samples amount to 6.73 ± 0.16 nb⁻¹ and 10.0 ± 0.22 nb⁻¹ in the p-going and Pb-going directions, respectively, and to 663 ± 15 μb^{-1} for Pb–Pb collisions after merging the 2015 and 2018 data samples. The quoted uncertainties are the systematic uncertainties, while the statistical ones are negligible.

The classification of the events in p–Pb collisions into centrality intervals is performed based on the energy deposited in the neutron calorimeters (ZN) of the ZDC in the direction of the Pb fragments. For each of these intervals, the average number of binary nucleon–nucleon collisions $\langle N_{\text{coll}} \rangle$ is obtained from the hybrid method described in Ref. [45]. The method relies on the assumption that the charged-particle multiplicity measured at midrapidity is proportional to the average number of nucleons participating in the interaction $\langle N_{\text{part}} \rangle$. The values of $\langle N_{\text{part}} \rangle$ for a given ZN-centrality class are calculated by scaling the average number of participants in MB collisions $\langle N_{\text{part}}^{\text{MB}} \rangle$, estimated by means of Glauber Monte Carlo (MC) [51, 52], with the ratio of the average charged-particle multiplicity measured at midrapidity for the ZN-centrality class to that in MB collisions. In the following, these values are denoted $\langle N_{\text{part}}^{\text{mult}} \rangle$ to indicate this assumption. The corresponding number of binary collisions is then obtained as $\langle N_{\text{coll}}^{\text{mult}} \rangle = \langle N_{\text{part}}^{\text{mult}} \rangle - 1$. The associated uncertainty is evaluated using different approaches as described in Ref. [52]. The resulting values of $\langle N_{\text{coll}}^{\text{mult}} \rangle$ and their uncertainties are summarised in Table 1. In Pb–Pb collisions, the centrality is determined from the distribution of the signal amplitude in the V0 arrays and is expressed in percentages of the total hadronic cross section. The collisional geometrical properties $\langle N_{\text{part}} \rangle$, $\langle N_{\text{coll}} \rangle$, and the nuclear overlap function $\langle T_{\text{AA}} \rangle$ of the different centrality intervals are obtained via a Glauber model fit to the V0 signal amplitude distribution. The Glauber model is also used to determine the so-called anchor point below which the centrality determination is not reliable. The values of $\langle T_{\text{AA}} \rangle$ in Pb–Pb collisions at $\sqrt{s_{\text{NN}}} = 5.02$ TeV are given in Table 2 for the centrality classes considered in this work.

The muon track candidates reconstructed in the events passing the requirements described above are selected according to the following criteria. A fiducial selection is applied on the track pseudorapidity, requiring it to be in the interval $-4 < \eta_{\text{lab}}^{\mu} < -2.5$ to remove the particles at the edge of the spectrometer

acceptance. An additional selection on the polar angle measured at the end of the front absorber, of $170^\circ < \theta_{\text{abs}} < 178^\circ$, rejects the tracks crossing the high-density region of the front absorber, where they experience significant multiple scatterings. The contamination by tracks not pointing to the nominal interaction vertex, mostly originating from beam–gas interactions and secondary particles produced in the front absorber, is efficiently removed by exploiting the correlation between the track momentum p and its distance of closest approach (DCA) to the vertex (i.e., the distance to the primary vertex of the track trajectory projected on the plane transverse to the beam axis). Being subject to multiple scatterings in the front absorber, the DCA of particles produced in the collision follows a Gaussian distribution, with a sigma depending on the material crossed and being proportional to the inverse of the momentum p . Background tracks, on the other hand, have on average a DCA larger than about 40 cm, independently of their momentum. A selection on the product of the track momentum with its DCA ($p \times \text{DCA}$) allows the suppression of this background source down to a negligible level. Finally, the muon identification is performed by matching the track reconstructed in the tracking system with a track segment in the trigger stations. The track in the tracking system is extrapolated to the trigger stations, and a χ^2 -based criterion determines the quality of the matching.

3 Analysis strategy

3.1 Overview

The W^\pm bosons are detected through their muonic decay channel via the $W^- \rightarrow \mu^- \bar{\nu}_\mu$ and $W^+ \rightarrow \mu^+ \nu_\mu$ processes following the method described in Ref. [20]. Since ALICE is not a hermetic detector, one cannot reconstruct the missing transverse energy due to the presence of a neutrino in the final state. The signal extraction is therefore performed from the single muon p_T distribution, excluding the $p_T^\mu < 10$ GeV/ c interval where the signal-to-background ratio is very small. One can distinguish three main contributions to the inclusive spectrum, namely muons originating from the decay of W^\pm , Z^0/γ^* , and heavy-flavour (charm and beauty) hadrons. The signal extraction procedure relies on templates, which are generated by means of MC simulations, and are used to fit the measured muon p_T distributions according to

$$f(p_T) = N_{\text{HF}}^{\text{raw}} f_{\text{HF}}(p_T) + N_{\mu^\pm \leftarrow W^\pm}^{\text{raw}} \left(f_{\mu^\pm \leftarrow W^\pm}(p_T) + R \times f_{\mu^\pm \leftarrow Z^0/\gamma^*}(p_T) \right), \quad (1)$$

where f_{HF} , $f_{\mu^\pm \leftarrow W^\pm}$, and $f_{\mu^\pm \leftarrow Z^0/\gamma^*}$ are the templates accounting for muons from heavy-flavour hadrons, W^\pm -boson, and Z^0/γ^* decays, respectively. The number of muons from heavy-flavour hadrons and W^\pm -boson decays ($N_{\text{HF}}^{\text{raw}}$ and $N_{\mu^\pm \leftarrow W^\pm}^{\text{raw}}$) are free parameters of the fit, while the number of muons from Z^0/γ^* decays is forced to be proportional to that of W^\pm decays according to the ratio R of their production cross sections as predicted by MC simulations using the POWHEG event generator [53].

3.2 MC simulations

The production of muons from W^\pm and Z^0/γ^* decays was simulated by means of MC simulations at NLO using the POWHEG event generator [53]. Since POWHEG is only intended for the simulation of hard partonic scattering processes, it was matched to PYTHIA 6 [54] for parton shower description. In the simulations, the CT10 PDF set [55] was used along with the EPS09NLO [56] parametrisation of the nuclear modifications. In order to account for the isospin effect, which is of particular importance for the W^\pm -boson production yields, simulations of proton–proton (pp), proton–neutron (pn), neutron–proton (np), and also neutron–neutron (nn) binary collisions for Pb–Pb, were performed. The total cross sections were obtained from the single pp, pn, np, and nn cross sections combined with weights proportional to the density of protons and neutrons in a Pb nucleus:

$$\frac{d^2 \sigma_{\text{NN}}^{\text{pPb}}}{dp_T dy} = \frac{Z}{A} \times \frac{d^2 \sigma_{\text{pp}}^{\text{pPb}}}{dp_T dy} + \frac{A-Z}{A} \times \frac{d^2 \sigma_{\text{pn}}^{\text{pPb}}}{dp_T dy}, \quad (2)$$

$$\frac{d^2\sigma_{NN}^{\text{PbPb}}}{dp_T dy} = \frac{Z^2}{A^2} \times \frac{d^2\sigma_{pp}^{\text{PbPb}}}{dp_T dy} + \frac{(A-Z)^2}{A^2} \times \frac{d^2\sigma_{nn}^{\text{PbPb}}}{dp_T dy} + \frac{Z(A-Z)}{A^2} \times \left(\frac{d^2\sigma_{pn}^{\text{PbPb}}}{dp_T dy} + \frac{d^2\sigma_{np}^{\text{PbPb}}}{dp_T dy} \right), \quad (3)$$

where Eq. 2 indicates the combination in p–Pb collisions and Eq. 3 the combination for the Pb–Pb system.

The contribution of muons from heavy-flavour hadron decays was simulated using the Fixed-Order Next-to-Leading-Log (FONLL) approach [57]. The FONLL calculations were performed with the NNPDF3.1 PDF set [35], without accounting for nuclear modifications. In p–Pb collisions, the nuclear effects mainly affect the production of heavy-flavour hadrons at low p_T , typically below 5 GeV/c [58], and are expected to be negligible in the p_T interval studied in this paper. In the analysis of the Pb–Pb data sample, the FONLL predictions were multiplied by the nuclear modification factor R_{AA} of muons from heavy-flavour hadron decays, taken from simulations performed within the EPOS framework [59] in the interval $10 < p_T^\mu < 50$ GeV/c, fitted with a first-order polynomial function and further extrapolated to high p_T . The FONLL predictions were then used as inputs for the MC generation of muons from heavy-flavour hadron decays.

The MC simulations were performed by using the GEANT3 transport code [60] combined with a detailed simulation of the detector response and taking into account the time evolution of the detector configuration and alignment effects. In the high- p_T^μ region studied in this analysis ($p_T^\mu > 10$ GeV/c), the tracks are weakly bent, the alignment of the tracking chambers is therefore of utmost importance for the track reconstruction. The absolute positions of the chambers were first measured with photogrammetry before the data taking. The relative positions of the detection elements were then refined with a combination of reconstructed tracks in data samples recorded with and without magnetic field using a modified version of the MILLEPEDE package [61], up to a precision of about 100 μm . The estimated residual misalignment is then taken into account in the MC simulations. In addition, one may expect a misalignment of the spectrometer in its entirety, which is addressed by studying the track-to-cluster residual distribution in the data and the simulation. The simulation of the tracking chamber response relies on a data-driven parametrisation of the measured resolution of the clusters associated to a track. The distribution of the difference between the cluster and the track positions in each chamber is described using extended Crystal Ball (CB) [62] functions, with parameters tuned on data. The CB parametrisation is then used to reproduce the smearing of the track parameters in the simulations. A global misalignment of the detector is mimicked by shifting the distribution of the track deviations in the magnetic field. The sign of the shift is reverted for positive and negative tracks, and according to the magnetic field polarity. Its magnitude was tuned in order to reproduce the observed difference in the p_T^μ distribution of positive and negative tracks.

3.3 Signal extraction and efficiency correction

Examples of the W^- and W^+ signal extraction are shown in Fig. 1 and 2 for p–Pb and Pb–Pb collisions, respectively. In p–Pb collisions, an example is given for each combination of the colliding beam configuration and the charge of the muon. In Pb–Pb collisions, examples are given for the two charges of the muon, in the full centrality interval or for the 10% most central collisions. For both collision systems, the decay of W^\pm bosons becomes the dominant contribution for p_T^μ above 25 or 30 GeV/c. The fits to Eq. 1 are found to describe well the data, although at high p_T^μ they tend to underestimate the muon yield in some configurations. This difference between the data and the fit occurs in a p_T^μ interval where the number of muons is small, and has a negligible impact on the signal extraction.

The signal extraction procedure is affected by different sources of systematic uncertainties, which are related to the knowledge of the shape of the templates. The effect of this uncertainty on the extracted W^\pm -boson yield was estimated by studying the fit stability with reasonable variations of these shapes. The W^\pm -boson and Z^0/γ^* templates were generated using the CT10 [55] and CTEQ6 [33] PDF sets paired with either EPS09 [56] or EKS98 [63] nPDF, both at either LO or NLO. Varying the inputs of the simulations leads to different values of the R factor of Eq. 1, estimated from the same simulations.

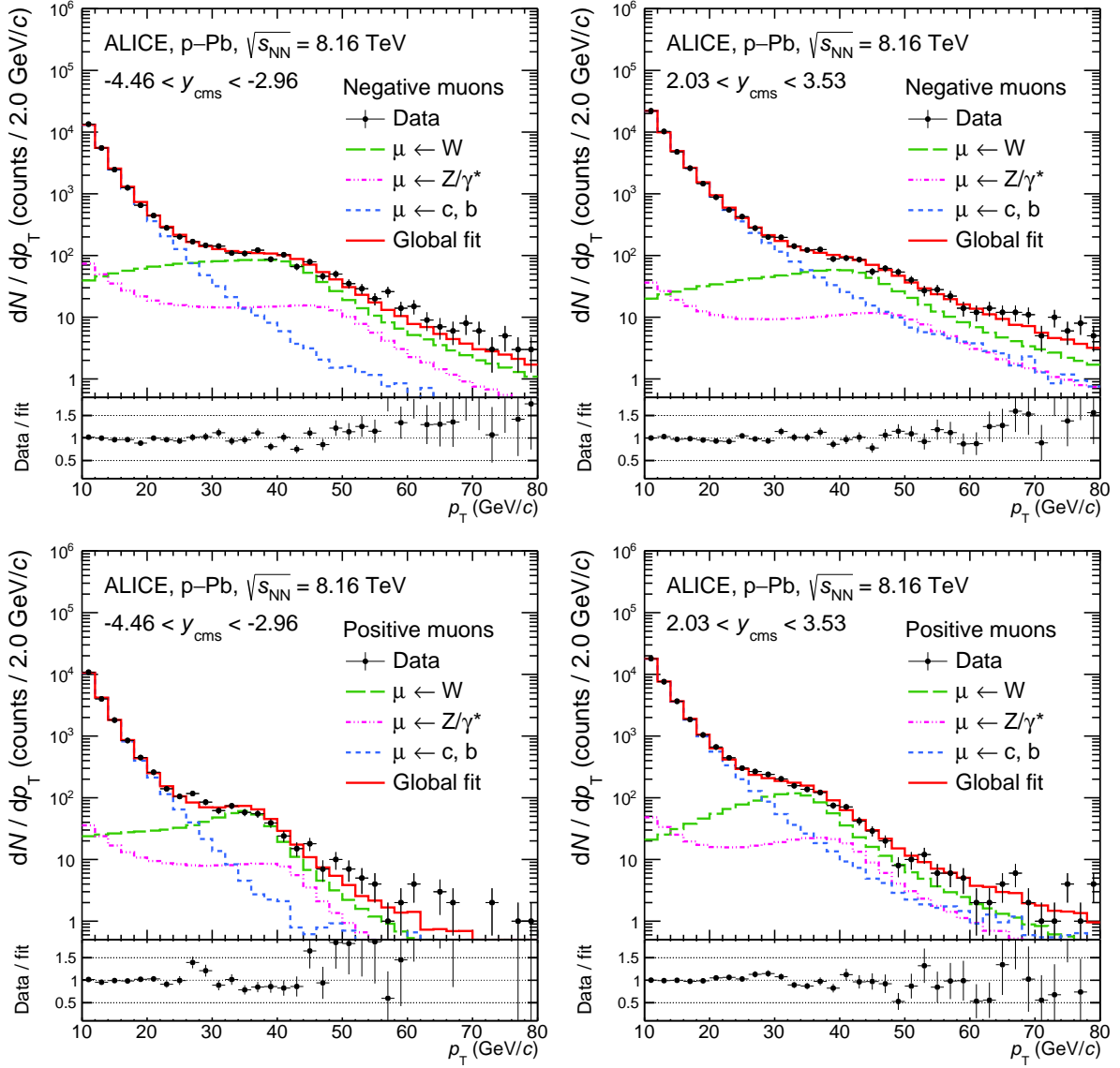


Figure 1: Inclusive transverse momentum distribution of negative (top) and positive (bottom) muons at backward (left) and forward (right) rapidity in p–Pb collisions at $\sqrt{s_{NN}} = 8.16$ TeV. The results of the fit to the inclusive spectrum using a combination of MC templates is shown as a continuous line, the green, pink and blue dashed lines representing the contributions of the W^\pm -, Z^0/γ^* - and heavy-flavour hadron decay muons, respectively. The bottom panels show the ratio of the data to the fit result.

The template accounting for muons from heavy-flavour hadron decays was computed by varying the FONLL calculations used as input within their uncertainties, originating from the choice of quark masses, factorisation and renormalisation scales, and from the uncertainty on the PDFs. In Pb–Pb collisions the uncertainty due to the p_T^μ extrapolation of the R_{AA} of muons from heavy-flavour hadron decays was estimated using different functional forms, as well as fitting the ALICE measurement of the R_{AA} between $7 < p_T^\mu < 20$ GeV/c and extrapolating the fit result to high p_T . The difference between the various extrapolations is taken as systematic uncertainty on the FONLL weighting procedure. For the simulation of the detector response, the tuning parameter of the global shift was varied within the uncertainty on its determination. The CB parameters for the cluster resolution, obtained from the data-driven method, were replaced by a set of parameters evaluated from simulations. The fit range was varied by moving the lower limit of the p_T^μ interval between 10 and 20 GeV/c and the higher limit between 50 and 80 GeV/c.

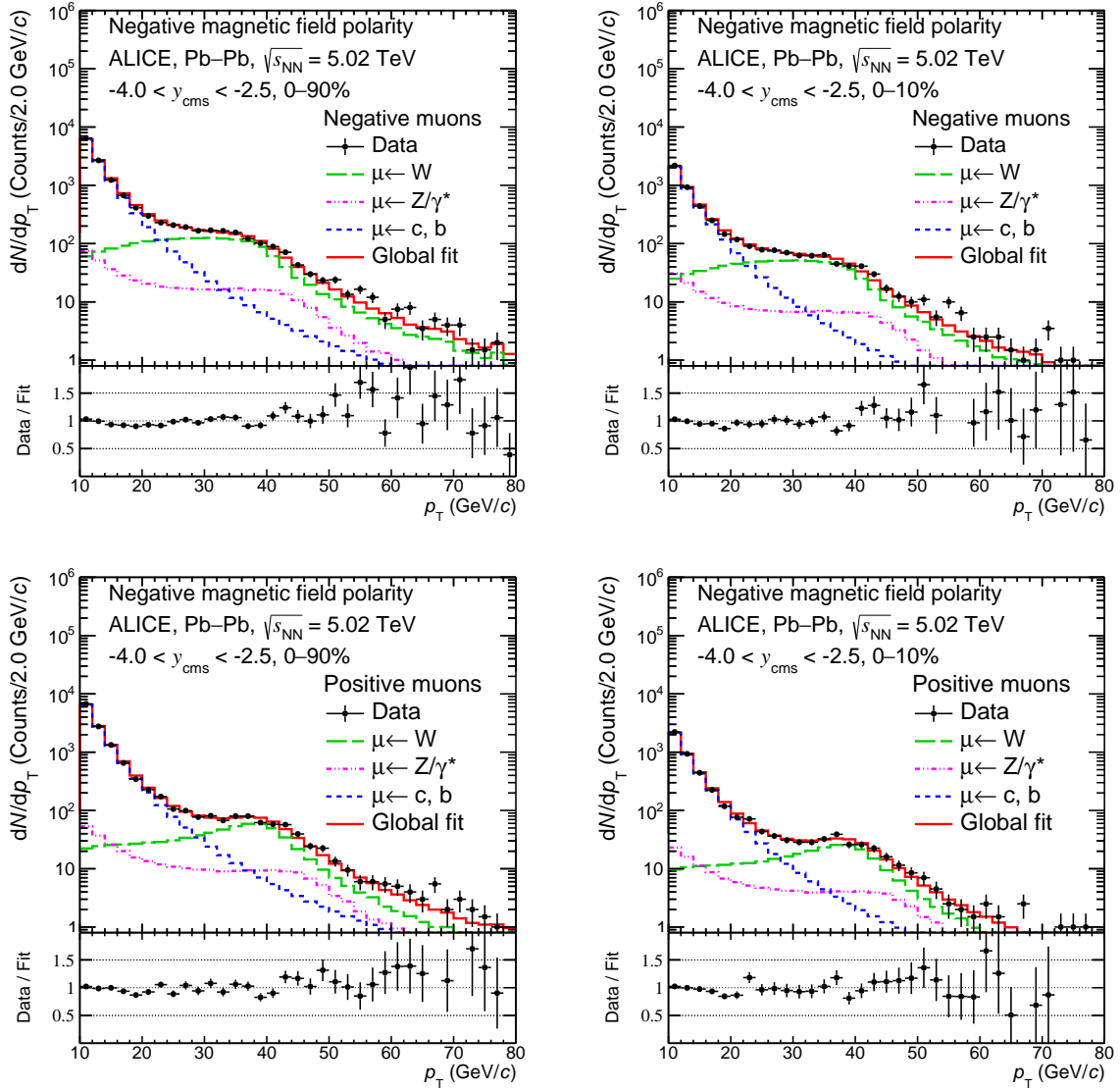


Figure 2: Inclusive transverse momentum distribution of negative (top) and positive (bottom) muons for the 0–90% (left) and 0–10% (right) centrality intervals in Pb–Pb collisions at $\sqrt{s_{NN}} = 5.02$ TeV. The results of the fit to the inclusive spectrum using a combination of MC templates is shown as a continuous line, the green, pink and blue dashed lines representing the contributions of the W^\pm -, Z^0/γ^* - and heavy-flavour hadron decay muons, respectively. The bottom panels show the ratio of the data to the fit result.

All the possible combinations of the variations were considered, each configuration yielding a value for $N_{\mu^\pm \leftarrow W^\pm}^{\text{raw}}$. The combined χ^2/ndf of the fits to the μ^- and μ^+ distributions was required to be smaller than 2 to ensure that only the configurations able to satisfactorily reproduce the data were kept. The final number of muons from W^\pm decays, and the associated statistical uncertainty, were obtained by averaging over the $N_{\mu^\pm \leftarrow W^\pm}^{\text{raw}}$ distribution obtained from all considered variations.

The extracted raw yield is corrected for the detection and reconstruction efficiency ε obtained from the simulations described in the previous section. The efficiency is estimated as the ratio of the number of reconstructed muons from W^\pm -boson decays, with the same selections as applied to the data, to the number of generated W^\pm -decay muons in the region of interest, that is the fiducial region defined by the selection on the muon $p_T^\mu > 10$ GeV/c, and the detector angular acceptance, $2.5 < y_{\text{cms}}^\mu < 4$. The

Table 3: Summary of systematic uncertainties affecting the W^\pm -boson measurements in p–Pb and Pb–Pb collisions. The values given for Pb–Pb collisions are for the combined 2015 and 2018 data samples. The ranges correspond to the largest variations found in differential analyses.

Source	Relative systematic uncertainty		
	p–Pb analysis	Pb–p analysis	Pb–Pb analysis
Signal extraction	5.9 – 8.8 %	3.8 – 7.3 %	2.9 – 3.3 %
- as a function of rapidity	3.9 – 14.3 %	2.5 – 22 %	—
- as a function of centrality	5.1 – 9.7 %	3.6 – 9.0 %	3.0 – 7.4 %
Tracking efficiency	0.5 %	1.0 %	1.5 %
Trigger efficiency		0.5 %	0.75 %
Trigger–tracker matching		0.5 %	0.5 %
Alignment		0.1 – 1.2 %	1.8 %
Normalisation factor	1.4 %	1.1 %	1.0 %
σ_{V0M}		1.9 %	2.0 %
$\langle N_{coll}^{mult} \rangle$	2.8 – 4.3 %		—
$\langle T_{AA} \rangle$		—	0.7 – 2.0 %

efficiency in p–Pb collisions amounts to 90% (91%) in the p-going configuration and 88% (89%) in the Pb-going one for μ^- (μ^+). In Pb–Pb collisions, the efficiency is additionally affected by the detector occupancy. This effect was taken into account by embedding the simulated signal into Pb–Pb data. The efficiency for the most central collisions is found to be 94% of the efficiency of the most peripheral collisions. The centrality-integrated efficiency for the 2015 period amounts to 83% and 81% for μ^- and μ^+ , respectively, while for the 2018 period the efficiency is 80% and 79% for μ^- and μ^+ , respectively. The efficiency has no significant dependence on p_T^μ , and decreases by about 9% from the most central to the largest rapidities.

3.4 Systematic uncertainties

The systematic uncertainties are summarised in Table 3. The signal extraction procedure described in the previous section yields a distribution of $N_{\mu^\pm \leftarrow W^\pm}^{raw}$ after the variation of the fit configuration and the simulation parameters. The dispersion (RMS) of the distribution was used as systematic uncertainty on the signal extraction. The uncertainty originating from the signal extraction procedure ranges from about 4% to 9% in the rapidity- and centrality-integrated studies. In the rapidity-differential measurements, for the largest rapidity intervals, the lower amount of signal reduces the stability of the fit such that the systematic uncertainty rises up to 22%.

The uncertainty of the efficiency computation is evaluated by varying the simulation environment. It was observed that, in the simulations, only the ability to properly reproduce the alignment conditions provides a significant source of uncertainty through the estimation of the CB tails parameters and the tuning of the parameter accounting for the global shift. The systematic uncertainty is taken as the largest difference between the efficiencies computed with all the possible configurations. The uncertainty on the tracking efficiency is obtained by considering the difference between the efficiencies obtained from data and MC simulations, using the redundancy of the tracking chamber information [48]. The uncertainty on the muon trigger efficiency is determined by propagating the uncertainty on the intrinsic efficiency of the individual trigger chambers, which is evaluated using a data-driven method based on the redundancy of the trigger chamber information [48]. The choice for the χ^2 value in defining the matching between the tracks in the tracking and trigger systems introduces an additional 0.5% uncertainty. The difference between the two methods for the computation of the normalisation, detailed in Section 2.2, is taken as its systematic uncertainty. The uncertainties on the σ_{V0M} values are taken from Refs. [49, 50] where their evaluation is detailed. Finally, the uncertainty on $\langle N_{coll}^{mult} \rangle$ in p–Pb collisions is evaluated as the difference with respect to the average number of binary collisions estimated using an alternative method based on

the multiplicity measured in the Pb-going direction [52]. In Pb–Pb collisions, the uncertainty on $\langle T_{\text{AA}} \rangle$ is estimated by varying the parameters of the Glauber model within their own uncertainties, adding in quadrature the maximum-to-average ratio of the upward and downward variations from all sources [52]. The total systematic uncertainty is obtained by summing all the considered sources in quadrature.

4 Results

4.1 p–Pb collisions

4.1.1 Production cross sections

The $\mu^\pm \leftarrow W^\pm$ rapidity-differential production cross section, uncorrected for the W-to-muon branching ratio BR, is evaluated as

$$\frac{d\sigma_{W^\pm \rightarrow \mu^\pm \nu_\mu}}{dy} = \frac{N_{\mu^\pm \leftarrow W^\pm}}{\Delta y \times \varepsilon \times \mathcal{L}_{\text{int}}}, \quad (4)$$

where $N_{\mu^\pm \leftarrow W^\pm}$ is the measured yield of muons from W^\pm decays, Δy is the width of the rapidity interval, ε is the efficiency correction factor, and \mathcal{L}_{int} the integrated luminosity. In p–Pb collisions at $\sqrt{s_{\text{NN}}} = 8.16$ TeV, the values of the corresponding production cross sections are reported in Table 4, where the Pb-going denomination refers to the backward rapidity interval $-4.46 < y_{\text{cms}}^\mu < -2.96$ and the p-going denomination to the forward interval $2.03 < y_{\text{cms}}^\mu < 3.53$.

Table 4: Rapidity-differential production cross sections of W^- and W^+ bosons measured from their muonic decays in p–Pb collisions at $\sqrt{s_{\text{NN}}} = 8.16$ TeV, for muons with $p_{\text{T}}^\mu > 10$ GeV/ c .

	$-4.46 < y_{\text{cms}}^\mu < -2.96$ (Pb-going)	$2.03 < y_{\text{cms}}^\mu < 3.53$ (p-going)
$W^- \rightarrow \mu^- \bar{\nu}_\mu$	105.4 ± 3.7 (stat) ± 5.2 (syst) nb	90.2 ± 4.8 (stat) ± 8.2 (syst) nb
$W^+ \rightarrow \mu^+ \nu_\mu$	37.1 ± 2.1 (stat) ± 2.9 (syst) nb	120.8 ± 5.2 (stat) ± 7.7 (syst) nb

The production cross section is shown as a function of rapidity, in the Pb-going and p-going directions and for both charges of the W boson, in Fig. 3. The measurements are compared with several pQCD calculations, based on Monte Carlo for FeMtobarn processes (MCFM) [64] or Fully Exclusive W and Z production (FEWZ) [65] simulations. The MCFM and FEWZ codes enable the calculation of hard processes in hadronic collisions, involving heavy flavour and top quarks, electroweak bosons and the Higgs boson. The two codes were shown to produce similar predictions of the electroweak-boson production at NLO [66]. The nuclear modifications are computed using the CT14+EPPS16 [30], nCTEQ15WZ [36] and nNNPDF2.0 [32] parametrisations, as discussed in Section 1. To illustrate the effect of using the LHC data in the determination of nPDFs, predictions were also obtained from the nCTEQ15 set [31] in which no LHC data were included. In order to disentangle the effect of the nuclear modifications of the PDFs from other effects affecting the W^\pm -boson production, such as the isospin, predictions are shown for the CT14 PDF [67] without nuclear modifications. All calculations are performed at NLO, the proton and neutron contributions are weighted following the nucleon content of the Pb ion to reproduce the isospin dependence of the W^\pm -boson production.

Several effects affect the production of the W^- and W^+ bosons in p–Pb collisions. The isospin effect, originating from the difference in the quark content of the Pb nucleus to that of the proton, increases the production of W^- and decreases that of W^+ . The rapidity shift due to the asymmetric system pushes the forward rapidity range covered by the muon spectrometer, corresponding to the p-going configuration, towards midrapidity, where the production cross section is higher, and moves the backward rapidity range, in the Pb-going configuration, towards even larger rapidities where the production rate is reduced. Moreover, the production is affected by the helicity conservation. The weak interaction only couples left-handed fermions and right-handed antifermions. For angular momentum conservation, the outgoing

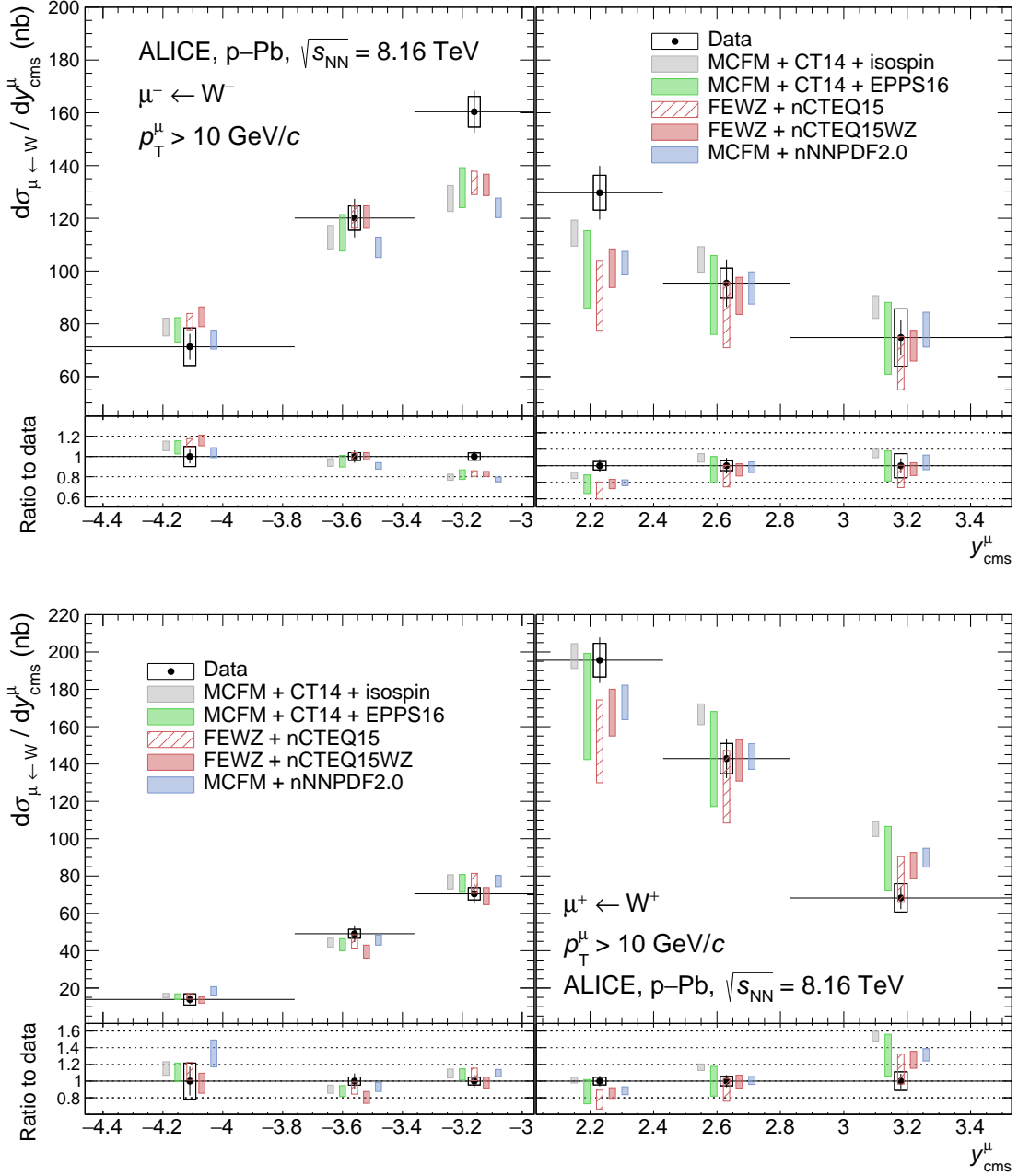


Figure 3: Production cross section of muons from W^- (top) and W^+ (bottom) decays as a function of rapidity for muons with $p_T^\mu > 10$ GeV/ c in p-Pb collisions at $\sqrt{s_{NN}} = 8.16$ TeV. The measurements are compared with predictions from several nPDF sets, as well as with calculations based on the CT14 PDF set [67] without nuclear modifications of the PDF. All the calculations include the isospin effect. The bottom panels show the ratio of the calculations to the measured production cross section. The horizontal bars correspond to the width of the rapidity intervals. The vertical bars and boxes indicate the statistical and systematic uncertainties, respectively. The data points are placed at the centres of the rapidity intervals, while the theory predictions are horizontally shifted for better visibility.

fermion μ^- (antifermion μ^+) follows the direction of the incoming quark q (antiquark \bar{q}). The production cross section is then maximum when the outgoing lepton (antilepton) goes in the direction of the incoming quark (antiquark). As a result, W^- bosons produced at large absolute rapidities will preferably emit μ^- in their momentum direction and W^+ will preferably emit μ^+ in the opposite direction. In the latter case, the muon reaches the large rapidity covered by the spectrometer only if the boson is produced in the opposite direction, at even larger rapidities where the production quickly drops. Finally, the nuclear modifications of the PDFs affect the production at backward and forward rapidities differently. At backward rapidity, the Bjorken- x interval accessible with the ALICE measurements is influenced by the anti-shadowing and EMC effects, yielding an enhancement and a reduction of the production, respectively. On the other hand, the forward rapidity interval is fully contained within the Bjorken- x region dominated by shadowing, resulting in a suppression of the parton densities. Although in most cases the effects just discussed tend to cancel each other, at least to some extent, they globally act towards a suppression of the W^+ production at backward rapidities.

The measured W^+ production cross section is in fair agreement with the model predictions, whereas some tension appears in the description of the rapidity dependence of the W^- production cross section, for small values of the absolute rapidity. For W^+ bosons measured at forward rapidities, corresponding to the shadowing region at low Bjorken- x , the measurement favours predictions including the nuclear modifications of the PDFs. The discrepancy with the free-nucleon PDF calculation is especially visible at large positive rapidities where the deviation from the CT14-only prediction reaches 3.5σ , with the statistical and systematic uncertainties combined quadratically. The precision of the measurement is better than that of the theory, highlighting its ability to provide further constraints for nPDF sets. The comparison between the nCTEQ15 and nCTEQ15WZ predictions shows the impact of the LHC data on the determination of the nPDFs, whose uncertainties are substantially reduced despite the addition of three new free parameters in nCTEQ15WZ, corresponding to the parametrisation of the strange-quark nPDF. The nNNPDF group, which has adopted a methodology based on machine learning for the determination of the nPDF, yields predictions with the smallest uncertainties in the forward rapidity region, corresponding to very low Bjorken- x values. The four models including nuclear modifications are in good agreement with each other, although some discrepancies are present between nCTEQ15WZ and nNNPDF2.0 calculations at backward rapidities.

The CMS Collaboration also measured the production of the W^\pm bosons via the muonic decay channel in p–Pb collisions at $\sqrt{s_{\text{NN}}} = 8.16$ TeV from a data sample with an integrated luminosity of $173.4 \pm 6.1 \text{ nb}^{-1}$ [15]. The production was measured at midrapidity, in the interval $|\eta_{\text{lab}}^\mu| < 2.4$, complementary to the ALICE measurement at large rapidities. A stronger selection was applied on the muon transverse momentum at $p_T^\mu > 25 \text{ GeV}/c$, a direct comparison is therefore not possible. However, the two measurements can be compared through their agreement with theoretical calculations. Figure 4 shows the ratio of the measurements to pQCD calculations performed including the isospin effect and using either the CT14 PDF set (without nuclear modifications) or the CT14 set with the EPPS16 nPDFs.

The measurements of ALICE extend to large rapidities the measurements of the CMS Collaboration in the central region, and support the trend observed at the edge of the CMS rapidity acceptance. The calculations including the EPPS16 nPDFs provide a better description of the data over the whole rapidity interval as compared to the predictions with the CT14 PDFs without nuclear effects, especially for the W^+ boson.

4.1.2 Lepton charge asymmetry

The production of W^- and W^+ bosons is significantly dependent on the light-quark content of the nucleus. The study of the asymmetry in their production therefore provides a sensitive probe of the up and down nPDF as well as the down-to-up ratio in the nucleus. In this regard, the lepton charge asymmetry

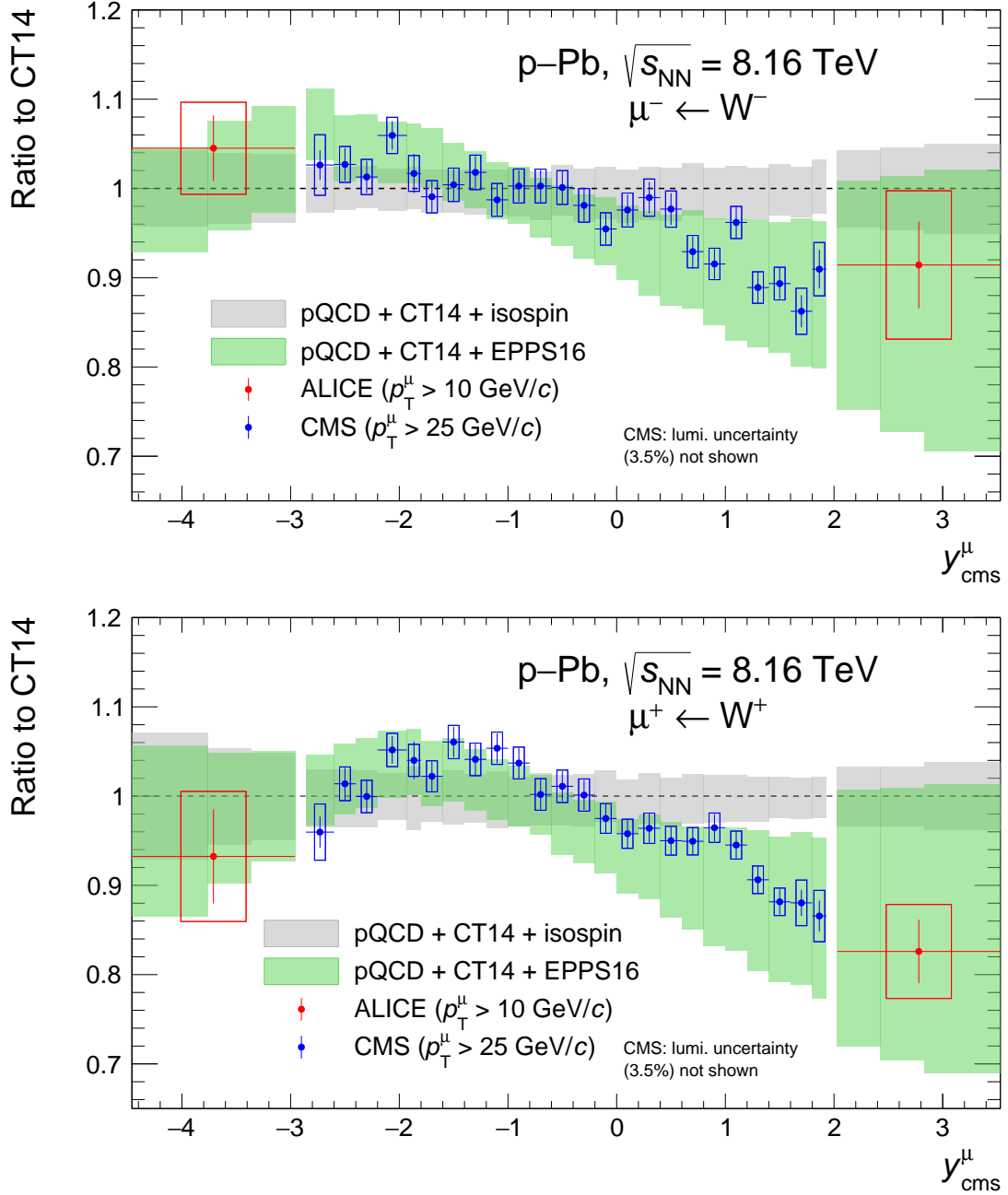


Figure 4: Ratio to CT14 [67] predictions of the production of muons from W^- (top) and W^+ (bottom) decays measured in p-Pb collisions at $\sqrt{s_{NN}} = 8.16$ TeV by the ALICE and CMS [15] Collaborations. The measured ratio is compared to the one obtained from pQCD calculations with CT14+EPPS16 [30]. All the calculations include the isospin effect. The grey band around the line at unity indicates the uncertainty on the calculations with CT14 PDFs.

A_{ch} can be defined as

$$A_{\text{ch}} = \frac{N_{\mu^+\leftarrow W^+}^{\text{corr}} - N_{\mu^-\leftarrow W^-}^{\text{corr}}}{N_{\mu^+\leftarrow W^+}^{\text{corr}} + N_{\mu^-\leftarrow W^-}^{\text{corr}}}, \quad (5)$$

where $N_{\mu^-\leftarrow W^-}^{\text{corr}}$ and $N_{\mu^+\leftarrow W^+}^{\text{corr}}$ are the number of muons from W^- and W^+ decays, respectively, extracted from the data and corrected for the detection and reconstruction efficiency. Part of the experimental uncertainties, such as the trigger and tracking efficiencies, cancels in the calculation of the asymmetry. The theoretical precision is also increased, e.g. through the cancellation of the uncertainties due to the pQCD scales. It should be noted that the lepton charge asymmetry might be much more sensitive to the baseline PDF than to its nuclear modifications [28], possibly enabling the study of the free-nucleon PDF in heavy-ion collisions.

The measured lepton charge asymmetries integrated over $p_{\text{T}}^\mu > 10$ GeV/ c in the rapidity intervals covered by the muon spectrometer for the two colliding beam configurations are:

$$A_{\text{ch}}^{\text{Pb-going}} = -0.479 \pm 0.046 \text{ (stat)} \pm 0.056 \text{ (syst)}, \quad A_{\text{ch}}^{\text{p-going}} = 0.145 \pm 0.014 \text{ (stat)} \pm 0.021 \text{ (syst)}.$$

The measured A_{ch} as a function of rapidity is shown in Fig. 5. Consistently with the up and down quark compositions of the proton and Pb ion, the A_{ch} shows a predominance of W^- bosons at backward rapidities, in the Pb-going direction, and of W^+ at forward rapidities. At very large positive rapidities, the lepton charge asymmetry becomes negative, which indicates a suppression of the W^+ production. This suppression could be a consequence of the helicity conservation affecting the muonic decay of the boson, or a sharper slope of the up quark PDF in the shadowing region towards low Bjorken- x . The A_{ch} is compared with predictions from pQCD calculations with the CT14+EPPS16, nCTEQ15WZ, and nNNPDF2.0 PDFs sets, as well as with the CT14 PDF set for free nucleons. The calculations are performed at NLO and the same treatment of the isospin as for the production cross section is applied. The models reproduce the data well at backward rapidity, although a small tension is seen for the most central rapidity interval in which the theory predicts an increase of the charge asymmetry, while the measurement is independent of centrality within uncertainties. At forward rapidities, the model predictions and the measurements are in qualitative agreement, both showing a reduction of the charge asymmetry towards higher rapidities. However, the decrease seen in the data is notably larger than that in calculations, and it is interesting to note the sign inversion of the measured charge asymmetry, while the calculations stay positive over the whole forward rapidity interval. In the largest rapidity interval, the models are all lying more than 5σ above the measurement.

4.1.3 Nuclear modification factor

In p–Pb collisions, the nuclear modification factor R_{pPb} , integrated over centrality, is calculated as

$$R_{\text{pPb}} = \frac{1}{A} \times \frac{d\sigma_{W^\pm \rightarrow \mu^\pm \nu_\mu}^{\text{pPb}}/dy_{\text{cms}}^\mu}{d\sigma_{W^\pm \rightarrow \mu^\pm \nu_\mu}^{\text{pp}}/dy_{\text{cms}}^\mu}. \quad (6)$$

It evaluates the deviation between the measured production cross section in p–Pb collisions and the one expected from a superposition of uncorrelated pp collisions. It should be noted that for electroweak bosons, the R_{pPb} is a peculiar quantity. It is affected by the isospin effect, and as a consequence, expectation values for R_{pPb} can deviate from unity even in the absence of nuclear effects, such as the nuclear modification of the PDFs. Since no measurement of the W^\pm -boson production in pp collisions at $\sqrt{s} = 8.16$ TeV is available, the R_{pPb} presented here relies on theoretical calculations for the pp production cross section $\sigma_{W^\pm \rightarrow \mu^\pm \nu_\mu}^{\text{pp}}$. The simulations are performed with the procedure discussed in Section 3, using POWHEG [53] interfaced with PYTHIA 6 [54] for the event generation and CT10 [55] for the proton PDF. It should be mentioned that the LHCb Collaboration has shown that the available models, including CT10, are able to describe well the production of W^\pm bosons in pp collisions at similar

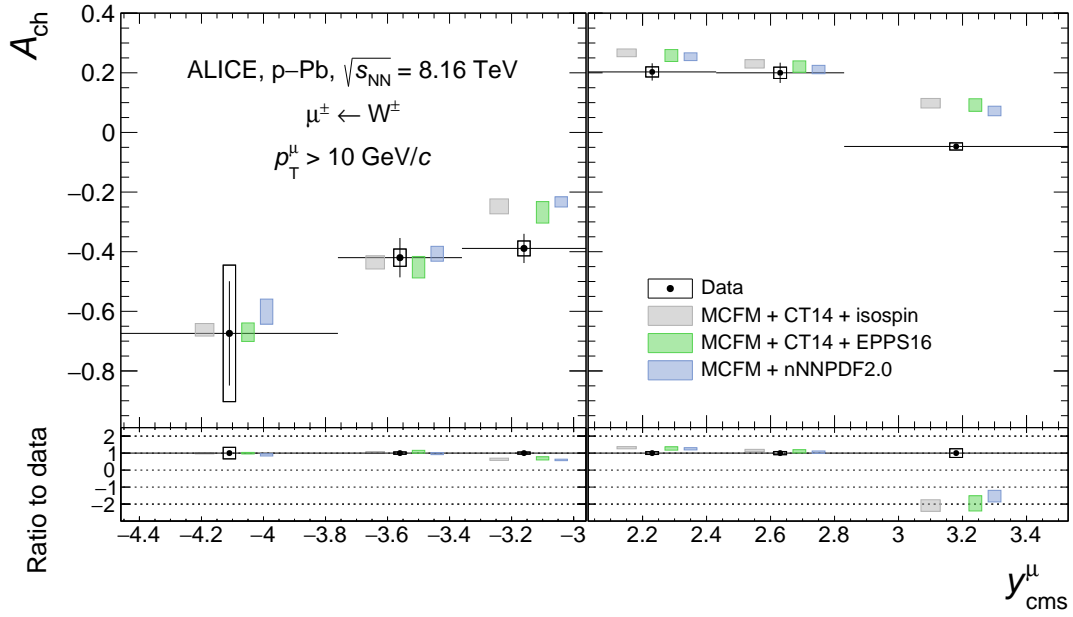


Figure 5: Lepton charge asymmetry for muons from W[±]-boson decays with $p_T^\mu > 10$ GeV/c in p–Pb collisions at $\sqrt{s_{NN}} = 8.16$ TeV. The measurements are compared with predictions from pQCD calculations with several nPDF sets as well as with calculations based on the CT14 PDF [67] without nuclear modifications. All the calculations include the isospin effect. The bottom panels show the ratio of the calculated to the measured asymmetry. The horizontal bars correspond to the width of the rapidity intervals. The vertical bars and boxes indicate the statistical and systematic uncertainties, respectively. The data points are placed at the centres of the rapidity intervals while the theory points are horizontally shifted for better visibility.

Table 5: Nuclear modification factors of the production of W[−] and W⁺ bosons measured in their muonic decays in p–Pb collisions at $\sqrt{s_{NN}} = 8.16$ TeV, for muons with $p_T^\mu > 10$ GeV/c. The pp reference cross sections are taken from simulations using the POWHEG [53] generator and CT10 PDF [55]. The quoted uncertainties correspond to the statistical and systematic uncertainties on the p–Pb measurement, and to the asymmetric systematic uncertainty on the pp reference, respectively.

	Pb-going ($-4.46 < y_{\text{cms}}^\mu < -2.96$)	p-going ($2.03 < y_{\text{cms}}^\mu < 3.53$)
$R_{\text{pPb}}(W^- \rightarrow \mu^- \bar{\nu}_\mu)$	$1.620 \pm 0.057 \pm 0.079^{+0.092}_{-0.062}$	$0.888 \pm 0.047 \pm 0.080^{+0.060}_{-0.039}$
$R_{\text{pPb}}(W^+ \rightarrow \mu^+ \nu_\mu)$	$0.643 \pm 0.036 \pm 0.051^{+0.046}_{-0.031}$	$0.793 \pm 0.034 \pm 0.051^{+0.048}_{-0.037}$

rapidities and energies [68]. The associated uncertainty was evaluated by varying the strong coupling constant α_s within its uncertainties and using CTEQ6.6 [69] as an alternative PDF set, summing the sources in quadrature. The values of the R_{pPb} obtained for the W[−]- and W⁺-boson production integrated over $p_T^\mu > 10$ GeV/c and the rapidity intervals covered by the muon spectrometer for the two colliding beam configurations are reported in Table 5.

The measured R_{pPb} is shown in Fig. 6 as a function of rapidity, where it is compared with predictions from the same models, and obtained using the same framework, as for the asymmetry A_{ch} . It should be noted that the nNNPDF2.0 predictions rely on a different baseline PDF, employing NNPDF3.1 [35] instead of the CT14 model used in the calculations with EPPS16 nPDFs. For both charges of the boson, the measured R_{pPb} is independent of y at backward rapidities, within the uncertainties. This trend is satisfactorily reproduced by the models for the W⁺ boson. For the W[−] boson however, a significant rapidity dependence is seen in the two calculations, which underestimate the measured value in the

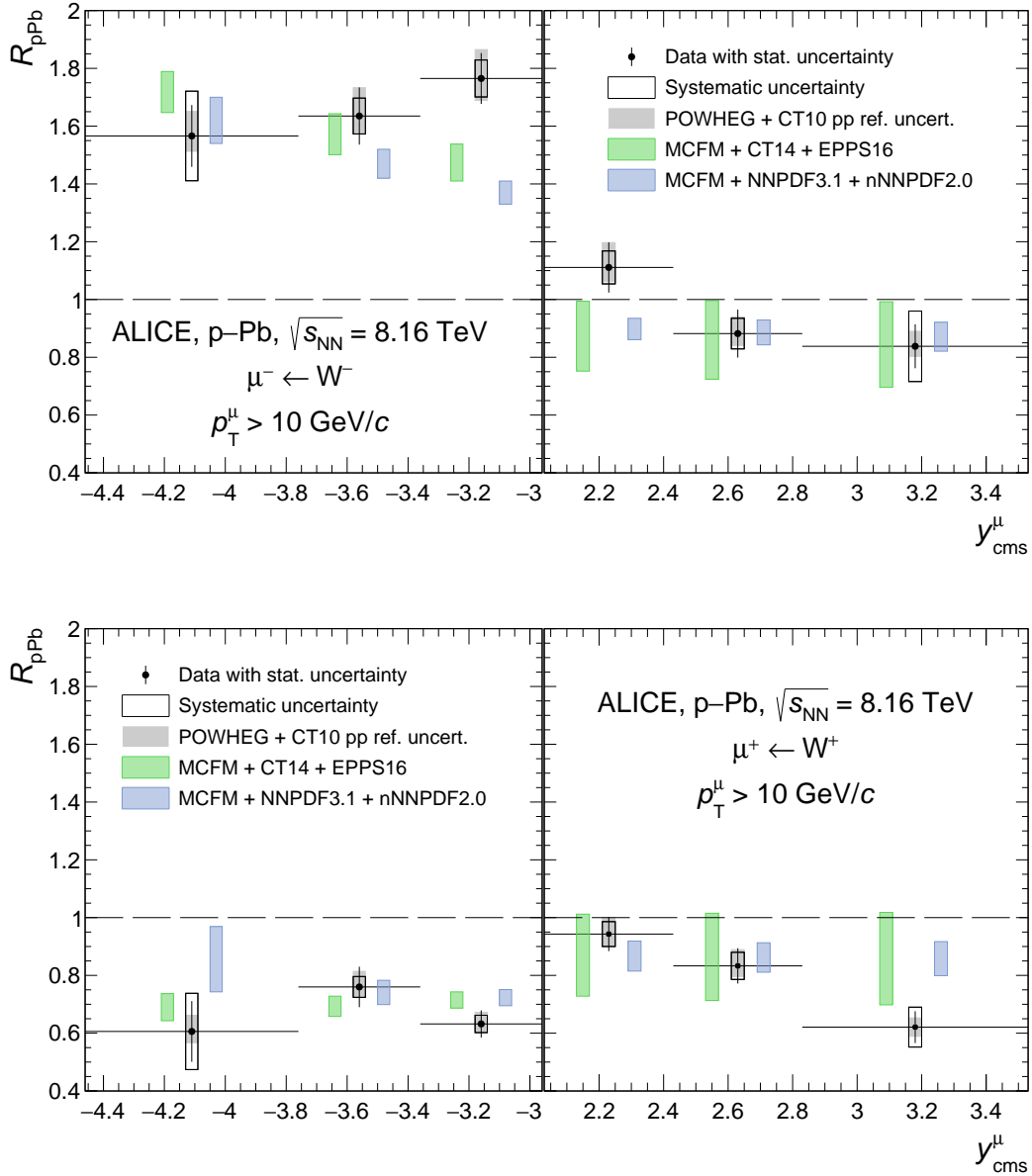


Figure 6: Nuclear modification factor R_{pPb} for muons from W^- (top) and W^+ (bottom) decays with $p_T^\mu > 10$ GeV/c in p-Pb collisions at $\sqrt{s_{NN}} = 8.16$ TeV. The measurements are compared with predictions from pQCD calculations with several nPDF sets. The horizontal bars correspond to the width of the rapidity bins. The vertical bars and boxes indicate the statistical and systematic uncertainties respectively. The grey bands indicate the uncertainty on the pp production cross section. The data points are placed at the centres of the rapidity intervals while the theory points are horizontally shifted for better visibility.

most central interval. At forward rapidities, the measured R_{pPb} decreases for the two charges while the calculations show a flat behaviour. This creates a tension with the calculations in the intervals closest to midrapidity for the W^- boson, where the models underestimate the measurement, and in the largest rapidity interval for the W^+ boson where the nNNPDF2.0 model overestimates the data.

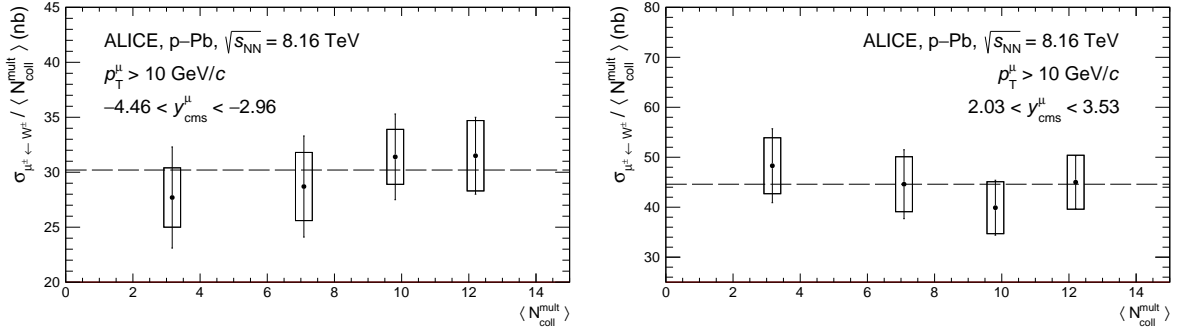


Figure 7: Combined yield of muons from W⁻ and W⁺ decays with $p_{\text{T}}^{\mu} > 10$ GeV/ c , normalised by the average number of binary nucleon–nucleon collisions $\langle N_{\text{coll}}^{\text{mult}} \rangle$ in p–Pb collisions at $\sqrt{s_{\text{NN}}} = 8.16$ TeV in the Pb-going (left) and p-going (right) configurations. The bars and boxes correspond to statistical and systematic uncertainties respectively. The horizontal dashed line indicates the central value of the yield normalised to $\langle N_{\text{coll}}^{\text{mult}} \rangle$ measured for the 0–100% centrality interval.

4.1.4 Production as a function of the collision centrality

The production of muons from W[±]-boson decays is studied as a function of the collision centrality. Electroweak-boson production occurs in hard scattering processes, during the initial stages of the collision, and is expected to scale with the number of binary nucleon–nucleon collisions, provided that the evaluation of the centrality is unbiased. As mentioned in Section 2, and in order to avoid the bias in multiplicity-based centrality estimators, the classification in centrality intervals is performed based on the energy deposited by the spectator (non-interacting) nucleons in the neutron zero-degree calorimeters (ZN) in the Pb-going side. The study of the centrality dependence of the W[±]-boson yield can therefore also serve as a test bench for the centrality estimation.

In order to maximise the amount of signal in each centrality class, the W⁻ and W⁺ yields are combined. The cross section normalised to the average number of nucleon–nucleon collisions, $\langle N_{\text{coll}}^{\text{mult}} \rangle$, is then calculated as

$$\frac{1}{\langle N_{\text{coll}}^{\text{mult}} \rangle} \times \frac{N_{\text{W}^{\pm}}^i}{\mathcal{L}_{\text{int}} \times f_{\text{MB}}^i \times \epsilon}, \quad (7)$$

where $\langle N_{\text{coll}}^{\text{mult}} \rangle$ is the average number of binary nucleon–nucleon collisions, $N_{\text{W}^{\pm}}^i$ is the number of muons from W[±] decays in a given centrality class i , and f_{MB}^i is the fraction of MB-triggered events in the centrality class i to those in the full centrality range (0–100%). The cross sections for the two colliding beam configurations, normalised to $\langle N_{\text{coll}}^{\text{mult}} \rangle$ and averaged over centrality, amount to:

$$\begin{aligned} -4.46 < y_{\text{cms}}^{\mu} < -2.96 : & \quad \sigma_{\mu^{\pm} \leftarrow \text{W}^{\pm}} / \langle N_{\text{coll}}^{\text{mult}} \rangle = 30.2 \pm 2.0 \text{ (stat)} \pm 2.8 \text{ (syst) nb,} \\ 2.03 < y_{\text{cms}}^{\mu} < 3.53 : & \quad \sigma_{\mu^{\pm} \leftarrow \text{W}^{\pm}} / \langle N_{\text{coll}}^{\text{mult}} \rangle = 44.6 \pm 3.3 \text{ (stat)} \pm 5.1 \text{ (syst) nb.} \end{aligned}$$

The normalised cross sections are shown as a function of $\langle N_{\text{coll}}^{\text{mult}} \rangle$ in Fig. 7. The horizontal dashed line in the figure indicates the central value of the centrality-averaged measurement. The measured yield divided by $\langle N_{\text{coll}}^{\text{mult}} \rangle$ is found to be independent of centrality within uncertainties.

4.2 Pb–Pb collisions

4.2.1 Production cross sections and lepton charge asymmetry

In Pb–Pb collisions at $\sqrt{s_{\text{NN}}} = 5.02$ TeV, the production cross section and lepton charge asymmetry of muons from W[±]-boson decays are evaluated as in p–Pb collisions, from Eqs. 4 and 5. The VOM amplitude is used to estimate the centrality of the collision. The production cross sections for W⁻ and

W^+ bosons in the 0–90% centrality class are

$$\sigma_{W^- \rightarrow \mu^- \bar{\nu}_\mu} = 18.7 \pm 0.7 \text{ (stat)} \pm 0.6 \text{ (syst)} \mu\text{b}, \quad \sigma_{W^+ \rightarrow \mu^+ \nu_\mu} = 7.0 \pm 0.4 \text{ (stat)} \pm 0.2 \text{ (syst)} \mu\text{b}.$$

In the left panel of Fig. 8, these values are compared with pQCD calculations using the CT14 [67], the CT14+EPPS16 combination [30, 67], and nNNPDF2.0 [32] PDF sets, all accounting for the isospin of the Pb–Pb system. In the Pb–Pb collision system, one cannot disentangle the high and low Bjorken- x ranges, as it was possible in p–Pb collisions. The comparison of the production for positively and negatively charged bosons shows the effect of the isospin, since the up- and down-quark densities in the Pb nucleus favour the production of W^- and suppress that of W^+ . The measured cross sections are lower than the predictions with the CT14 PDFs for free nucleons, suggesting a significant effect due to nuclear modifications of the PDFs on the W^\pm -boson production in Pb–Pb collisions. The calculations including the EPPS16 and nNNPDF2.0 nuclear modifications are consistent with the data within uncertainties. As it was observed in the predictions in p–Pb collisions, the nNNPDF2.0 calculations have significantly smaller uncertainties.

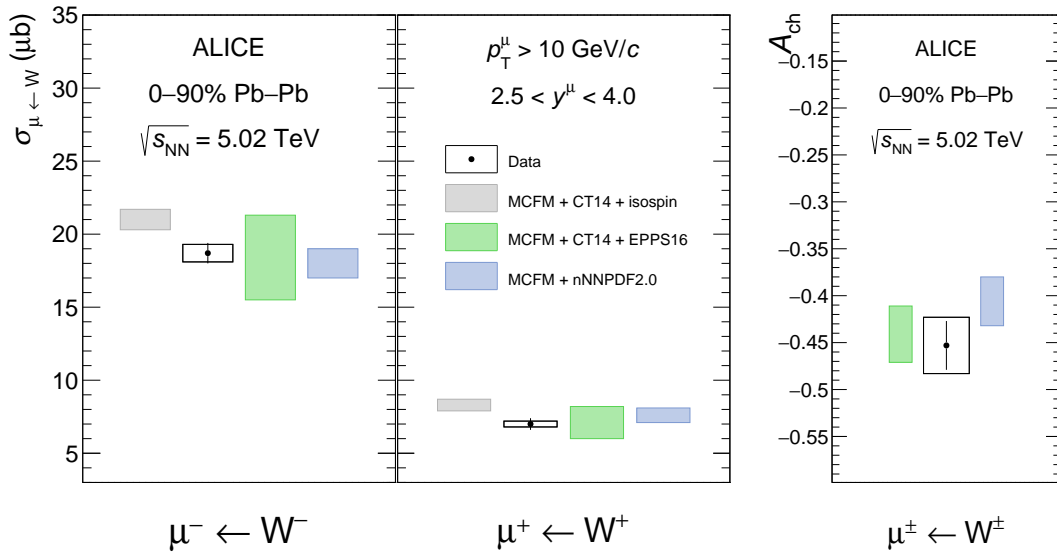


Figure 8: Production cross section (left panel) and lepton charge asymmetry (right panel) of the $W^\pm \rightarrow \mu^\pm \nu_\mu$ processes for the 0–90% centrality class, for muons with $p_T^\mu > 10$ GeV/ c and $2.5 < y_{\text{cms}}^\mu < 4.0$, in Pb–Pb collisions at $\sqrt{s_{NN}} = 5.02$ TeV. The measured cross sections and the asymmetry are compared with predictions using the CT14+EPPS16 [30, 67] combination, nNNPDF2.0 [32] nPDF model, as well as calculations with the CT14 [67] PDF without nuclear corrections. All the calculations include the isospin effect. The vertical bars and boxes around the data points indicate the statistical and systematic uncertainties, respectively.

The lepton charge asymmetry in the 0–90% centrality interval is measured to be

$$A_{\text{ch}} = -0.453 \pm 0.026 \text{ (stat)} \pm 0.030 \text{ (syst)}.$$

In the right panel of Fig. 8, this observable is compared with pQCD calculations using the CT14+EPPS16 [30] and nNNPDF2.0 [32] nPDFs. Both models describe well the measured value. The partial cancellation of uncertainty in the A_{ch} has a remarkable effect on the EPPS16 prediction, as the theoretical uncertainties are now similar to that in the data and nNNPDF2.0 calculation.

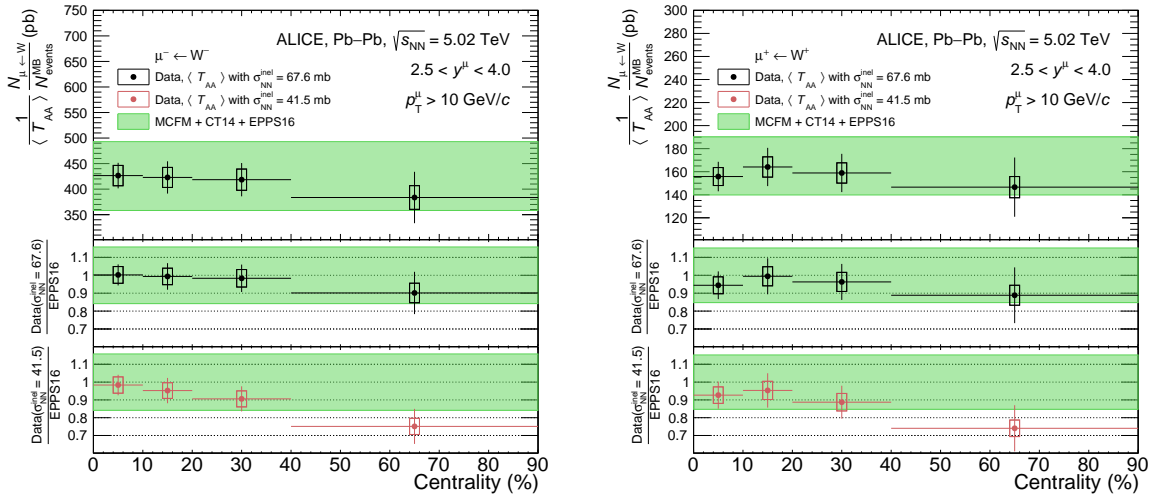


Figure 9: $\langle T_{AA} \rangle$ -scaled yield of muons from W^- (left) and W^+ (right) decays in Pb–Pb collisions at $\sqrt{s_{NN}} = 5.02$ TeV for muons with $p_T^\mu > 10$ GeV/ c and $2.5 < y_{cms}^\mu < 4.0$. In the top panels the yield is compared with pQCD calculations using the CT14 PDF [67] as baseline and implementing the EPPS16 [30] nuclear modifications. The ratio to theory of the measured yield normalised with $\langle T_{AA} \rangle$ evaluated with $\sigma_{NN}^{inel} = 67.6$ mb and 47.5 mb is shown in the middle and bottom panels, respectively (see the text for details). The horizontal bars indicate the width of the centrality intervals, the vertical bars and boxes correspond to the statistical and systematic uncertainties, respectively. The band indicate the uncertainty on the theoretical computations.

4.2.2 Normalised yield as a function of the collision centrality

The normalised yield is obtained by dividing the yield of muons from W^\pm decays, $N_{\mu^\pm \leftarrow W^\pm}$, by the equivalent number of MB events N_{events}^{MB} , and then normalising to the average nuclear overlap function $\langle T_{AA} \rangle$ [52]:

$$\frac{1}{\langle T_{AA} \rangle} \times \frac{N_{\mu^\pm \leftarrow W^\pm}}{N_{events}^{MB}}. \quad (8)$$

In the 0–90% centrality class, the binary-scaled yield amounts to

$$\begin{aligned} N_{\mu^- \leftarrow W^-} / (N_{events}^{MB} \times \langle T_{AA} \rangle) &= 420.5 \pm 16.4 \text{ (stat)} \pm 18.0 \text{ (syst)} \text{ pb}, \\ N_{\mu^+ \leftarrow W^+} / (N_{events}^{MB} \times \langle T_{AA} \rangle) &= 158.5 \pm 8.2 \text{ (stat)} \pm 6.9 \text{ (syst)} \text{ pb}. \end{aligned}$$

The W^\pm -boson yield normalised to $\langle T_{AA} \rangle$ as a function of the collision centrality is shown in Fig. 9 for both charges of the boson. The $\langle T_{AA} \rangle$ -scaled yields are independent of centrality, as expected from the binary scaling of W^\pm -boson production in nuclear collisions assuming negligible centrality dependence of the shadowing. The measurements are compared with pQCD calculations using the CT14 [67] PDF combined with the EPPS16 [30] nuclear modifications. A good agreement with the theory is found for both charges of the boson.

The centrality dependence of the PDF modifications has been explored through impact-parameter dependent nPDFs [70, 71], but calculations of electroweak-boson production within this approach show a very limited dependence on the centrality, as reported in Ref. [22]. A possible centrality dependence of the production in terms of shadowing of the inelastic nucleon–nucleon cross section σ_{NN}^{inel} was proposed in Ref. [72]. In that study, the standard paradigm of extracting σ_{NN}^{inel} from pp data, is questioned as a potential source of bias. The re-evaluation of the inelastic cross section from ATLAS measurements of electroweak-boson production in Pb–Pb collisions [11, 12] yields $\sigma_{NN}^{inel} = 41.5_{-12.0}^{+16.2}$ mb, a value significantly lower than the one used for centrality determination in Pb–Pb collisions at $\sqrt{s_{NN}} = 5.02$ TeV

with ALICE, taken as $\sigma_{\text{NN}}^{\text{inel}} = 67.6 \pm 0.6$ mb [52]. This alternative value of the inelastic cross section is found to improve the agreement between the ATLAS data and the pQCD calculations.

The bottom panels of Fig. 9 show the centrality-dependent measurements obtained by normalising the yield with $\langle T_{\text{AA}} \rangle$ evaluated using the nuclear-suppressed inelastic cross section from Ref. [72]. The distributions show a significant centrality dependence, with the W[−] distribution deviating from the binary scaling. This alternative value of the inelastic cross section, which provides a better agreement between pQCD calculations and the ATLAS measurement in peripheral collisions, has the opposite effect here. The yield normalised to $\langle T_{\text{AA}} \rangle$ with $\sigma_{\text{NN}}^{\text{inel}} = 41.5$ mb shows a worse agreement with the theory than that with $\sigma_{\text{NN}}^{\text{inel}} = 67.5$ mb in the 40–90% centrality interval. The authors of Ref. [72] expect other effects to be possibly relevant in peripheral collisions, such as a possible centrality dependence of $\sigma_{\text{NN}}^{\text{inel}}$ and the neutron-skin effect, which could explain the tension with the data for peripheral collisions. It should be noted that the neutron skin effect would affect the production of W[−] and W⁺ bosons in opposite directions, enhancing the former and suppressing the latter, thus not substantially improving the description of the measurements.

Recent measurements of the $\langle T_{\text{AA}} \rangle$ -normalised yield of the Z⁰ boson [10, 12, 18, 19] have shown a decreasing trend for the most peripheral events, contradicting the binary-scaling assumption. This phenomenon has also been observed and studied by the ALICE Collaboration [73] for charged particle production. A possible explanation for this observation has been formulated in terms of event selection and geometry biases affecting peripheral events in the HG-PYTHIA model [74]. In order to compare it with the Pb–Pb measurements presented in this article, the R_{AA} for hard scatterings calculated with this model was scaled by the centrality-averaged, $\langle T_{\text{AA}} \rangle$ -normalised yields of W[−] and W⁺ bosons measured in the 0–90% centrality class. The resulting distributions are compared with the centrality-dependent measurements in Fig. 10. The scaled calculations are in good agreement with the data, although the small W[±] yield in peripheral collisions does not allow for a granularity fine enough in the 40–90% centrality interval to show, if any, a statistically significant decrease of the production in this region.

The ATLAS Collaboration measured the production of W[±] bosons in the electronic and muonic decay channels in Pb–Pb collisions at $\sqrt{s_{\text{NN}}} = 5.02$ TeV [11]. Their results are reported for the 0–80% centrality class and are extracted from a data sample corresponding to a total integrated luminosity of 0.49 nb^{−1}. The decay leptons are detected in the rapidity interval $|y| < 2.5$, allowing for a complete continuity with the ALICE measurement in $2.5 < y < 4.0$. Similarly to the CMS measurements presented in Section 4.1, the ATLAS Collaboration also applied a tighter selection on the lepton p_{T} , at 25 GeV/c, the comparison is thus performed by means of the ratio between the measured W[±]-boson yields and the predictions from two pQCD calculations, the first using the EPPS16 [30] nPDF set and the second using the CT14 [67] PDFs. The comparison as a function of rapidity is shown in the two panels of Fig. 11 for the two charges of the boson.

The ALICE measurements are lower by 2σ than the CT14 predictions and are described by EPPS16. The ATLAS data, instead, are better described by calculations without nPDF effects. This comparison motivated the study in Ref. [72] with a shadowing-induced reduction of the inelastic cross section, but other possible origins of the effect have also been proposed [75].

4.2.3 Nuclear modification factor

In the Pb–Pb analysis, the nuclear modification factor of muons from W[±]-boson decays is evaluated by dividing the $\langle T_{\text{AA}} \rangle$ -scaled yield by the W[±]-boson production cross section in pp collisions:

$$R_{\text{AA}} = \frac{1}{\langle T_{\text{AA}} \rangle} \times \frac{N_{\mu^{\pm} \leftarrow W^{\pm}}^{\text{MB}}}{\sigma_{\text{pp}}^{\mu^{\pm} \leftarrow W^{\pm}}}, \quad (9)$$

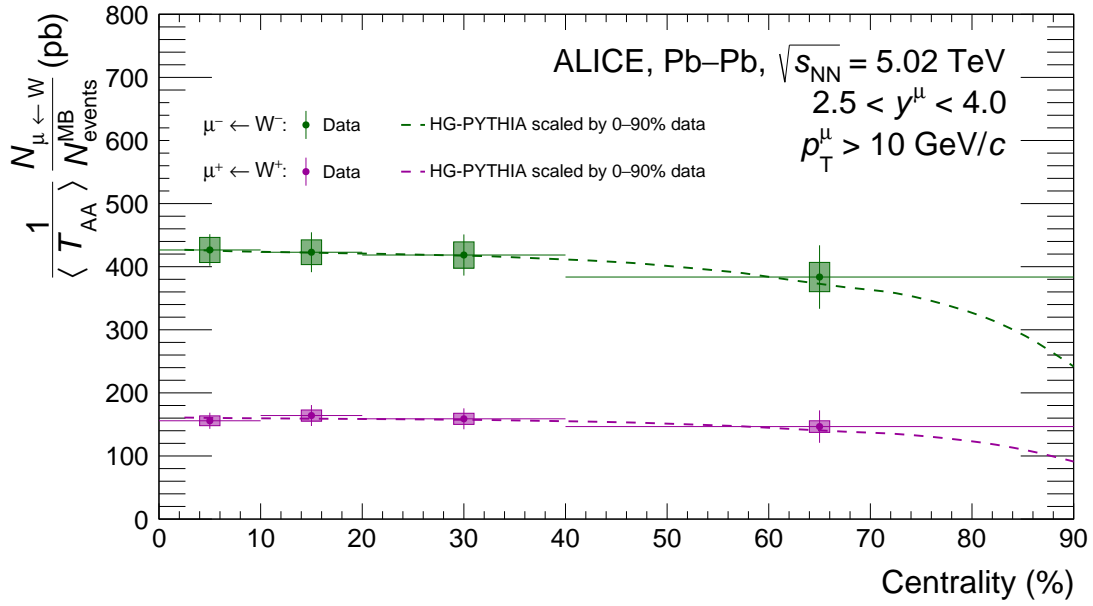


Figure 10: $\langle T_{AA} \rangle$ -scaled yield of muons from W^- and W^+ decays in Pb–Pb collisions at $\sqrt{s_{NN}} = 5.02$ TeV for muons with $p_T^\mu > 10$ GeV/ c and $2.5 < y_{\text{cms}}^\mu < 4.0$. The measured production is compared with HG-PYTHIA [74] calculations of the R_{AA} of hard scatterings scaled with the centrality-averaged production in 0–90% centrality, indicated as dashed lines. The horizontal bars correspond to the width of the centrality intervals, the vertical bars and boxes indicate the statistical and systematic uncertainties, respectively.

where $N_{\mu^\pm \leftarrow W^\pm}^{\text{MB}}$ is the number of muons from W^\pm decays per MB event, $\sigma_{pp}^{\mu^\pm \leftarrow W^\pm}$ is the $\mu^\pm \leftarrow W^\pm$ cross section in pp collisions, and $\langle T_{AA} \rangle$ is the average nuclear overlap function for the considered centrality class. As in p–Pb collisions, the pp production cross section and the associated uncertainty were obtained from POWHEG and PYTHIA 6 [53, 54] simulations using CT10 [55] for the proton PDF. For the 0–90% centrality interval, the R_{AA} of muons from W^- - and W^+ -boson decays are:

$$R_{AA}^{\mu^- \leftarrow W^-} = 1.32 \pm 0.05 \text{ (stat)} \pm 0.06 \text{ (syst)} \pm 0.14 \text{ (pp ref.)},$$

$$R_{AA}^{\mu^+ \leftarrow W^+} = 0.57 \pm 0.03 \text{ (stat)} \pm 0.02 \text{ (syst)} \pm 0.07 \text{ (pp ref.)}.$$

The production of W^- is enhanced, and that of W^+ is suppressed relative to pp collisions, as expected following the content in u and d quarks of the Pb nucleus.

The measured R_{AA} is shown in Fig. 12 as a function of centrality and for the 0–90% centrality class. The centrality-dependent measurement is compared with HG-PYTHIA [74] calculations of the R_{AA} of hard scatterings scaled with the measured value in 0–90% centrality. The centrality-averaged R_{AA} is compared with pQCD calculations, using the CT14 [67] PDFs for the proton and the nCTEQ15WZ [36] PDF set, or the NNPDF3.1+nNNPDF2.0 combination [32, 35] for the Pb nucleus. The calculations within the nCTEQ and NNPDF frameworks are only shown for the centrality-averaged value as they have no centrality dependence. Both models provide a good description of the measurement within uncertainties. It should be noted that this agreement is realised while the measurement and models use different PDF sets for the pp reference, and different codes for the pQCD calculations (POWHEG [53] for the experimental results, MCFM [64] and FEWZ [65] for the theoretical ones).

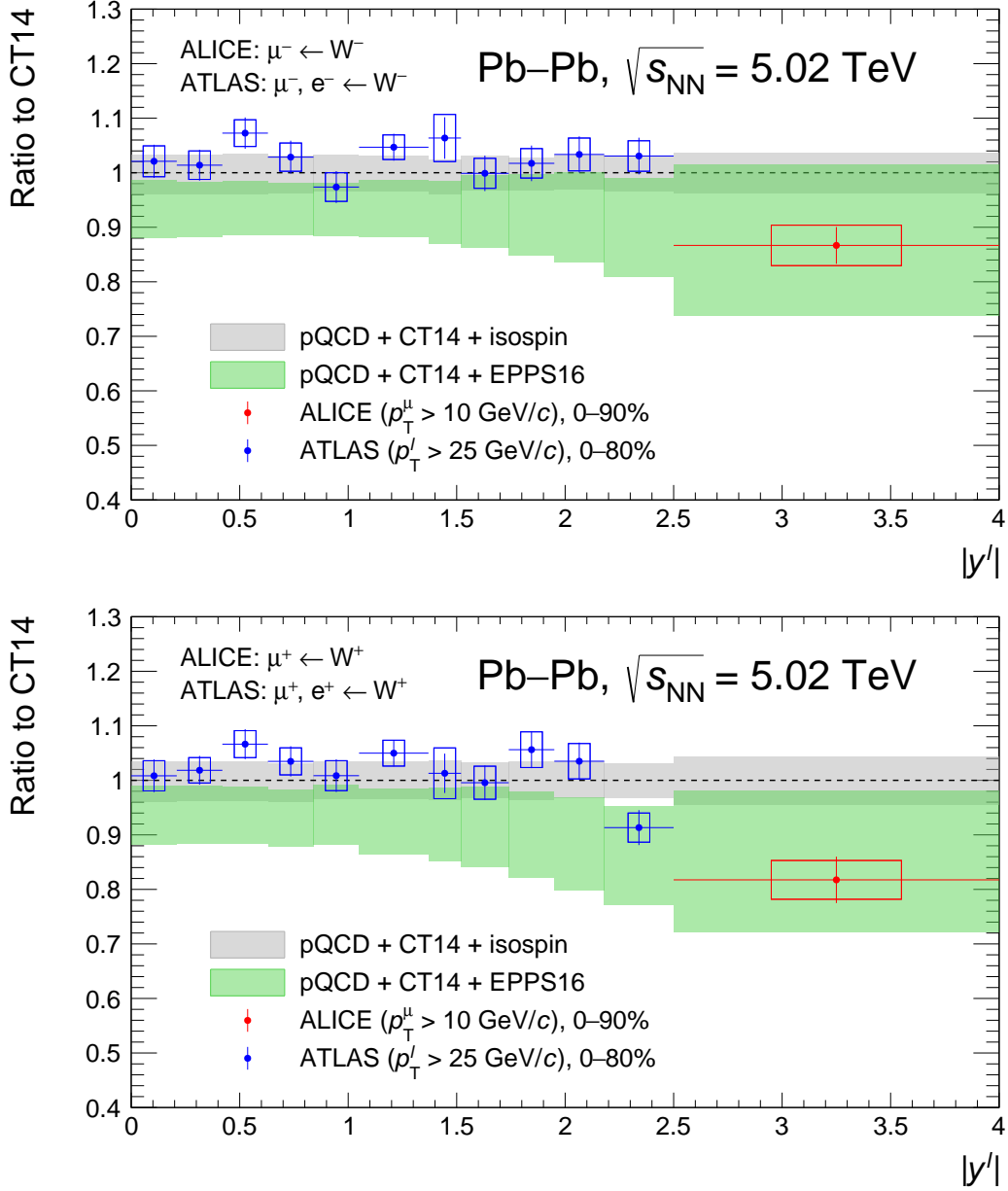


Figure 11: Ratio to pQCD calculations with CT14 PDFs [67] of the production of muons from W^- (top) and W^+ (bottom) decays measured as a function of rapidity in Pb-Pb collisions at $\sqrt{s_{NN}} = 5.02$ TeV by the ALICE and ATLAS [11] Collaborations. The ratio of EPPS16+CT14 [30] calculations to that of CT14-only calculations is also shown. The grey band around the line at unity indicates the uncertainty on the calculations with CT14 PDFs.

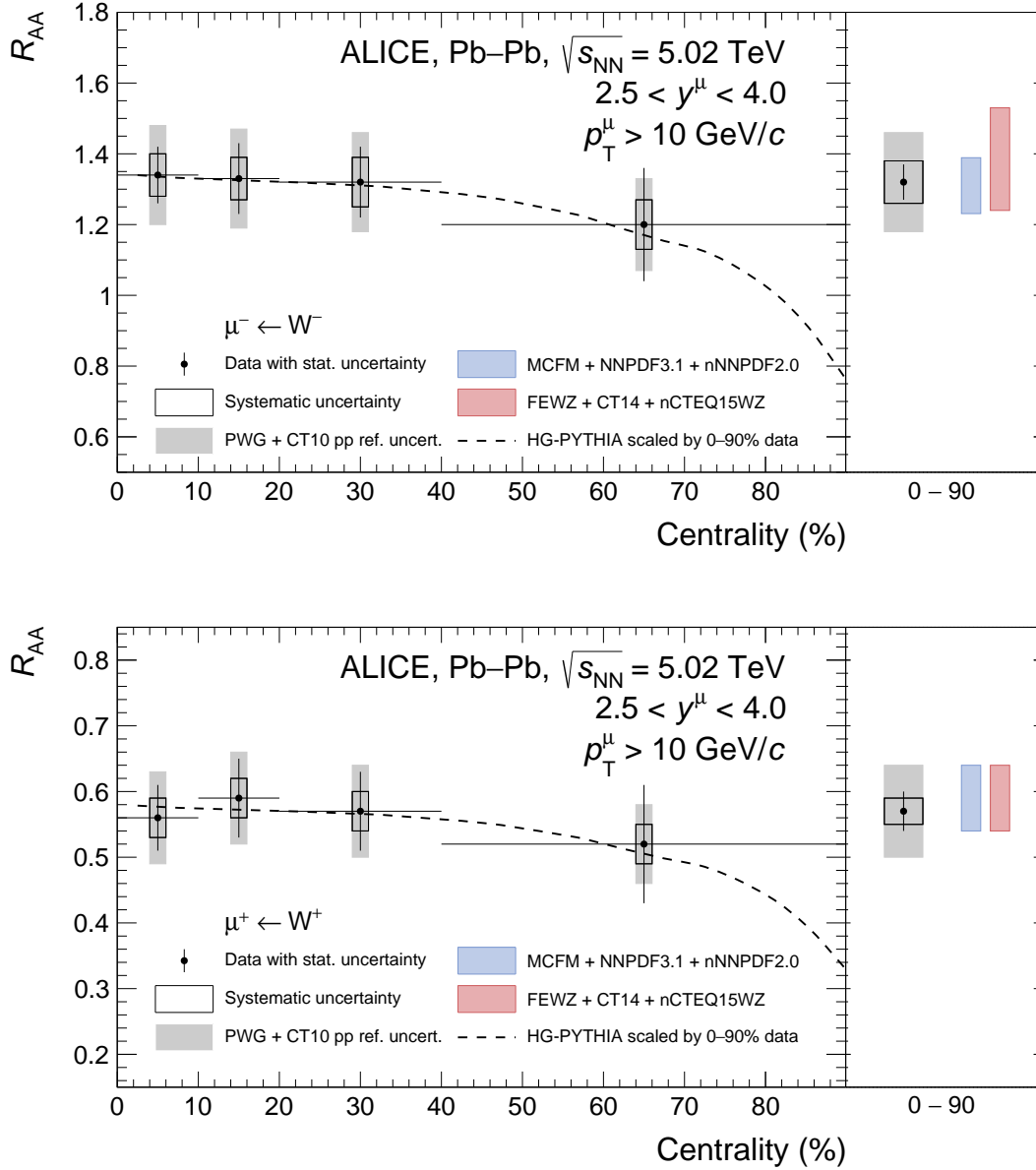


Figure 12: Nuclear modification factor of muons from W^- (top) and W^+ (bottom) decays in Pb-Pb collisions at $\sqrt{s_{NN}} = 5.02$ TeV, for muons with $p_T^\mu > 10$ GeV/c and $2.5 < y_{cms}^\mu < 4.0$, in different centrality intervals (left panels) and for the 0–90% range (right panels). The centrality-dependent distributions are compared with the dashed curve, corresponding to the HG-PYTHIA [74] model scaled with the measured R_{AA} in the 0–90% centrality interval. The centrality-averaged measurement is compared with CT14+nCTEQ15WZ [36, 67] and NNPDF3.1+nNNPDF2.0 [32, 35] calculations. The horizontal bars indicate the width of the centrality bins, the vertical bars and boxes correspond the statistical and systematic uncertainties on the Pb-Pb measurement, respectively. The grey boxes indicate the uncertainty on the pp reference cross section.

5 Summary

The measurements of the W[±]-boson production cross section, lepton charge asymmetry, nuclear modification factor, and yield normalised to the number of nucleon–nucleon collisions in p–Pb collisions at $\sqrt{s_{\text{NN}}} = 8.16$ TeV were reported, constituting the first results on the production of W[±] bosons at large rapidity at this energy, extending the measurement in p–Pb collisions at $\sqrt{s_{\text{NN}}} = 5.02$ TeV with a significant improvement of the precision. They were performed for muons with $p_{\text{T}}^{\mu} > 10$ GeV/*c* and in the rapidity intervals $-4.46 < y_{\text{cms}}^{\mu} < -2.96$ and $2.03 < y_{\text{cms}}^{\mu} < 3.53$, where the negative rapidity interval indicates the Pb-going side, and the positive one the p-going side. The results were compared with pQCD calculations, using the CT14 PDF set [67], and the EPPS16 [30], nNNPDF2.0 [32] and nCTEQ15 [31, 36] nPDF models. Some tensions are observed in the ability of the models to reproduce the data, notably in the rapidity dependence of the observables. Significant deviations from the free-nucleon PDF predictions, up to 3.5σ , are found at forward rapidity, corresponding to the shadowing region of the nuclear modifications at low Bjorken-*x*. The measurements in p–Pb collisions reported here can therefore provide significant constraints to the nPDF models and help reducing their uncertainties. They complement the measurements of the Z⁰-boson production performed at large rapidities by the ALICE Collaboration [22], where the statistical precision was too limited to draw any conclusion on the nuclear modifications. The comparison with the CMS measurements at midrapidity illustrates the complementarity of the LHC experiments in providing such results. The binary scaling of hard processes is observed, as the production cross sections in different centrality classes normalised to the average number of binary nucleon–nucleon collisions were found to be constant within uncertainties.

Similar measurements performed in Pb–Pb collisions at $\sqrt{s_{\text{NN}}} = 5.02$ TeV were also presented, for muons from W[±]-boson decays at large rapidity ($2.5 < y_{\text{cms}}^{\mu} < 4.0$) with $p_{\text{T}}^{\mu} > 10$ GeV/*c*, and for various centrality classes. The normalised yield as a function of centrality follows the binary scaling expected for a hard process in the absence of significant centrality dependence of the shadowing. Comparisons with pQCD calculations show the ability of the EPPS16, nCTEQ15WZ and nNNPDF2.0 nPDFs to reproduce the production cross section, lepton charge asymmetry and nuclear modification factor. The evaluation of the $\langle T_{\text{AA}} \rangle$ -normalised yield with the nuclear-suppressed inelastic nucleon–nucleon cross section $\sigma_{\text{NN}}^{\text{inel}}$ obtained from Ref. [72], which was found to improve the agreement between the ATLAS data and the EPPS16 model, yields a tension between the ALICE measurements and EPPS16 calculations for peripheral events which is not seen with the standard value of $\sigma_{\text{NN}}^{\text{inel}}$. The $\langle T_{\text{AA}} \rangle$ -scaled yield and the nuclear modification factor are found to be in good agreement with HG-PYTHIA [74] calculations of the R_{AA} of hard scatterings scaled with the value measured in 0–90% centrality, but the statistical limitation of the measurement does not allow to conclude on the decrease in peripheral events expected from this model. The measured $\langle T_{\text{AA}} \rangle$ -scaled yields are described by pQCD calculations with the EPPS16 nPDFs. These measurements support the conclusion derived from the measurement of the Z⁰-boson production in Pb–Pb collisions at $\sqrt{s_{\text{NN}}} = 5.02$ TeV [22], showing a suppression of the production of electroweak bosons due to the nuclear modifications of the PDF and the resulting deviations from calculations based on free-nucleon PDFs. Being the first measurement of the W[±] production in Pb–Pb collisions at large rapidity, this study provides important insights for further investigation of the centrality dependence of the nPDFs.

Acknowledgements

The authors would like to thank Hannu Paukkunen, Rabah Abdul Khalek and Aleksander Kusina for providing the various model calculations.

The ALICE Collaboration would like to thank all its engineers and technicians for their invaluable contributions to the construction of the experiment and the CERN accelerator teams for the outstanding performance of the LHC complex. The ALICE Collaboration gratefully acknowledges the resources and

support provided by all Grid centres and the Worldwide LHC Computing Grid (WLCG) collaboration. The ALICE Collaboration acknowledges the following funding agencies for their support in building and running the ALICE detector: A. I. Alikhanyan National Science Laboratory (Yerevan Physics Institute) Foundation (ANSL), State Committee of Science and World Federation of Scientists (WFS), Armenia; Austrian Academy of Sciences, Austrian Science Fund (FWF): [M 2467-N36] and Nationalstiftung für Forschung, Technologie und Entwicklung, Austria; Ministry of Communications and High Technologies, National Nuclear Research Center, Azerbaijan; Conselho Nacional de Desenvolvimento Científico e Tecnológico (CNPq), Financiadora de Estudos e Projetos (Finep), Fundação de Amparo à Pesquisa do Estado de São Paulo (FAPESP) and Universidade Federal do Rio Grande do Sul (UFRGS), Brazil; Bulgarian Ministry of Education and Science, within the National Roadmap for Research Infrastructures 2020;2027 (object CERN), Bulgaria; Ministry of Education of China (MOEC) , Ministry of Science & Technology of China (MSTC) and National Natural Science Foundation of China (NSFC), China; Ministry of Science and Education and Croatian Science Foundation, Croatia; Centro de Aplicaciones Tecnológicas y Desarrollo Nuclear (CEADEN), Cubaenergía, Cuba; Ministry of Education, Youth and Sports of the Czech Republic, Czech Republic; The Danish Council for Independent Research — Natural Sciences, the VILLUM FONDEN and Danish National Research Foundation (DNRF), Denmark; Helsinki Institute of Physics (HIP), Finland; Commissariat à l’Energie Atomique (CEA) and Institut National de Physique Nucléaire et de Physique des Particules (IN2P3) and Centre National de la Recherche Scientifique (CNRS), France; Bundesministerium für Bildung und Forschung (BMBF) and GSI Helmholtzzentrum für Schwerionenforschung GmbH, Germany; General Secretariat for Research and Technology, Ministry of Education, Research and Religions, Greece; National Research, Development and Innovation Office, Hungary; Department of Atomic Energy Government of India (DAE), Department of Science and Technology, Government of India (DST), University Grants Commission, Government of India (UGC) and Council of Scientific and Industrial Research (CSIR), India; National Research and Innovation Agency - BRIN, Indonesia; Istituto Nazionale di Fisica Nucleare (INFN), Italy; Japanese Ministry of Education, Culture, Sports, Science and Technology (MEXT) and Japan Society for the Promotion of Science (JSPS) KAKENHI, Japan; Consejo Nacional de Ciencia (CONACYT) y Tecnología, through Fondo de Cooperación Internacional en Ciencia y Tecnología (FONCICYT) and Dirección General de Asuntos del Personal Académico (DGAPA), Mexico; Nederlandse Organisatie voor Wetenschappelijk Onderzoek (NWO), Netherlands; The Research Council of Norway, Norway; Commission on Science and Technology for Sustainable Development in the South (COMSATS), Pakistan; Pontificia Universidad Católica del Perú, Peru; Ministry of Education and Science, National Science Centre and WUT ID-UB, Poland; Korea Institute of Science and Technology Information and National Research Foundation of Korea (NRF), Republic of Korea; Ministry of Education and Scientific Research, Institute of Atomic Physics, Ministry of Research and Innovation and Institute of Atomic Physics and University Politehnica of Bucharest, Romania; Ministry of Education, Science, Research and Sport of the Slovak Republic, Slovakia; National Research Foundation of South Africa, South Africa; Swedish Research Council (VR) and Knut & Alice Wallenberg Foundation (KAW), Sweden; European Organization for Nuclear Research, Switzerland; Suranaree University of Technology (SUT), National Science and Technology Development Agency (NSTDA), Thailand Science Research and Innovation (TSRI) and National Science, Research and Innovation Fund (NSRF), Thailand; Turkish Energy, Nuclear and Mineral Research Agency (TENMAK), Turkey; National Academy of Sciences of Ukraine, Ukraine; Science and Technology Facilities Council (STFC), United Kingdom; National Science Foundation of the United States of America (NSF) and United States Department of Energy, Office of Nuclear Physics (DOE NP), United States of America. In addition, individual groups or members have received support from: Marie Skłodowska Curie, Strong 2020 - Horizon 2020, European Research Council (grant nos. 824093, 896850, 950692), European Union; Academy of Finland (Center of Excellence in Quark Matter) (grant nos. 346327, 346328), Finland; Programa de Apoyos para la Superación del Personal Académico, UNAM, Mexico.

References

- [1] S. D. Drell and T.-M. Yan, “Massive Lepton-Pair Production in Hadron-Hadron Collisions at High Energies”, *Physical Review Letters* **25** (1970) 316–320.
- [2] A. H. Ajjath, G. Das, M. C. Kumar, P. Mukherjee, V. Ravindran, and K. Samanta, “Resummed Drell-Yan cross-section at N^3LL ”, *Journal of High Energy Physics* **10** (2020) 153, arXiv:2001.11377 [hep-ph].
- [3] **Particle Data Group**, P. Zyla, *et al.*, “Review of Particle Physics”, *Progress of Theoretical and Experimental Physics* **2020** (2020) 083C01. <https://pdg.lbl.gov/>.
- [4] C. Anastasiou, L. Dixon, K. Melnikov, and F. Petriello, “High-precision QCD at hadron colliders: Electroweak gauge boson rapidity distributions at next-to-next-to leading order”, *Physical Review D* **69** (2004) 094008, arXiv:hep-ph/0312266 [hep-ph].
- [5] S. Catani, L. Cieri, G. Ferrera, D. de Florian, and M. Grazzini, “Vector Boson Production at Hadron Colliders: A Fully Exclusive QCD Calculation at Next-to-Next-to-Leading Order”, *Physical Review Letters* **103** (2009) 082001, arXiv:0903.2120 [hep-ph].
- [6] J. Gao, L. Harland-Lang, and J. Rojo, “The structure of the proton in the LHC precision era”, *Physics Reports* **742** (2018) 1–121, arXiv:1709.04922 [hep-ph].
- [7] K. Kovarik, P. Nadolsky, and D. Soper, “Hadron structure in high-energy collisions”, *Reviews of Modern Physics* **92** (2020) 045003, arXiv:1905.06957 [hep-ph].
- [8] **ATLAS Collaboration**, G. Aad *et al.*, “Z boson production in p+Pb collisions at $\sqrt{s_{NN}} = 2.76$ TeV measured with the ATLAS detector”, *Physical Review C* **92** (2015) 044915, arXiv:1507.06232 [hep-ex].
- [9] **ATLAS Collaboration**, G. Aad *et al.*, “Measurement of the production and lepton charge asymmetry of W bosons in Pb+Pb collisions at $\sqrt{s_{NN}} = 2.76$ TeV with the ATLAS detector”, *European Physics Journal C* **75** (2015) 23, arXiv:1408.4674 [hep-ex].
- [10] **ATLAS Collaboration**, G. Aad *et al.*, “Measurement of Z boson Production in Pb+Pb Collisions at $\sqrt{s_{NN}} = 2.76$ TeV with the ATLAS Detector”, *Physical Review Letters* **110** (2013) 022301, arXiv:1210.6486 [hep-ex].
- [11] **ATLAS Collaboration**, G. Aad *et al.*, “Measurement of W^\pm boson production in Pb+Pb collisions at $\sqrt{s_{NN}} = 5.02$ TeV with the ATLAS detector”, *European Physical Journal C* **79** (2019) 935, arXiv:1907.10414 [nucl-ex].
- [12] **ATLAS Collaboration**, G. Aad *et al.*, “Z boson production in Pb+Pb collisions at $\sqrt{s_{NN}} = 5.02$ TeV measured by the ATLAS experiment”, *Physics Letters B* **802** (2020) 135262, arXiv:1910.13396 [nucl-ex].
- [13] **CMS Collaboration**, V. Khachatryan *et al.*, “Study of W boson production in pPb collisions at $\sqrt{s_{NN}} = 5.02$ TeV”, *Physics Letters B* **750** (2015) 565, arXiv:1503.05825 [nucl-ex].
- [14] **CMS Collaboration**, V. Khachatryan *et al.*, “Study of Z boson production in pPb collisions at $\sqrt{s_{NN}} = 5.02$ TeV”, *Physics Letters B* **759** (2016) 36, arXiv:1512.06461 [hep-ex].
- [15] **CMS Collaboration**, A. M. Sirunyan *et al.*, “Observation of nuclear modifications in W^\pm boson production in pPb collisions at $\sqrt{s_{NN}} = 8.16$ TeV”, *Physics Letters B* **800** (2020) 135048, arXiv:1905.01486 [hep-ex].

- [16] **CMS** Collaboration, S. Chatrchyan *et al.*, “Study of W boson production in PbPb and pp collisions at $\sqrt{s_{NN}} = 2.76$ TeV”, *Physics Letters B* **715** (2012) 66, arXiv:1205.6334 [nucl-ex].
- [17] **CMS** Collaboration, S. Chatrchyan *et al.*, “Study of Z boson production in PbPb collisions at $\sqrt{s_{NN}} = 2.76$ TeV”, *Physical Review Letters* **106** (2011) 212301, arXiv:1102.5435 [nucl-ex].
- [18] **CMS** Collaboration, S. Chatrchyan *et al.*, “Study of Z production in PbPb and pp collisions at $\sqrt{s_{NN}} = 2.76$ TeV in the dimuon and dielectron decay channels”, *Journal of High Energy Physics* **03** (2015) 022, arXiv:1410.4825 [nucl-ex].
- [19] **CMS** Collaboration, A. M. Sirunyan *et al.*, “Constraints on the initial state of PbPb collisions via measurements of Z boson yields and azimuthal anisotropy at $\sqrt{s_{NN}} = 5.02$ ”, *Physical Review Letters* **127** (2021) 102002, arXiv:2103.14089 [hep-ex].
- [20] **ALICE** Collaboration, J. Adam *et al.*, “ W and Z boson production in p–Pb collisions at $\sqrt{s_{NN}} = 5.02$ TeV”, *Journal of High Energy Physics* **02** (2017) 077, arXiv:1611.03002 [nucl-ex].
- [21] **ALICE** Collaboration, S. Acharya *et al.*, “Measurement of Z^0 -boson production at large rapidities in Pb–Pb collisions at $\sqrt{s_{NN}} = 5.02$ TeV”, *Physics Letters B* **780** (2018) 372–383, arXiv:1711.10753 [nucl-ex].
- [22] **ALICE** Collaboration, S. Acharya *et al.*, “ Z -boson production in p–Pb collisions at $\sqrt{s_{NN}} = 8.16$ TeV and Pb–Pb collisions at $\sqrt{s_{NN}} = 5.02$ TeV”, *Journal of High Energy Physics* **09** (2020) 076, arXiv:2005.11126 [nucl-ex].
- [23] **LHCb** Collaboration, R. Aaij *et al.*, “Observation of Z production in proton-lead collisions at LHCb”, *Journal of High Energy Physics* **09** (2014) 030, arXiv:1406.2885 [hep-ex].
- [24] N. Armesto, “Nuclear shadowing”, *Journal of Physics G* **32** (2006) R367–R394, arXiv:hep-ph/0604108 [hep-ph].
- [25] S. Malace, D. Gaskell, D. W. Higinbotham, and I. Cloet, “The Challenge of the EMC Effect: existing data and future directions”, *International Journal of Modern Physics E* **23** (2014) 1430013, arXiv:1405.1270 [nucl-ex].
- [26] A. Szczurek and A. Budzanowski, “Fermi motion and nuclear modification factor”, *Modern Physics Letters A* **19** (2004) 1669–1680, arXiv:nucl-th/0311025 [nucl-th].
- [27] B. Z. Kopeliovich, J. G. Morfin, and S. I., “Nuclear Shadowing in Electro-Weak Interactions”, *Progress in Particle and Nuclear Physics* **68** (2013) 314, arXiv:1208.6541 [hep-ph].
- [28] H. Paukkunen and C. A. Salgado, “Constraints for the nuclear parton distributions from Z and W production at the LHC”, *Journal of High Energy Physics* **03** (2011) 071, arXiv:1010.5392 [hep-ph].
- [29] Z. Conesa del Valle, “Vector bosons in heavy-ion collisions at the LHC”, *European Physical Journal C* **61** (2009) 729–733, arXiv:0903.1432 [hep-ex].
- [30] K. J. Eskola, P. Paakkinen, H. Paukkunen, and C. A. Salgado, “EPPS16: Nuclear parton distributions with LHC data”, *European Physical Journal C* **77** (2017) 163, arXiv:1612.05741 [hep-ph].
- [31] K. Kovarik *et al.*, “nCTEQ15 - Global analysis of nuclear parton distributions with uncertainties in the CTEQ framework”, *Physical Review D* **93** (2016) 085037, arXiv:1509.00792 [hep-ph].

- [32] R. A. Khalek, J. J. Ethier, J. Rojo, and G. van Weelden, “nNNPDF2.0: Quark Flavor Separation in Nuclei from LHC Data”, *Journal of High Energy Physics* **09** (2020) 183, arXiv:2006.14629 [hep-ph].
- [33] J. Pumplin, D. R. Stump, J. Huston, H. L. Lai, P. Nadolsky, and W. K. Tung, “New Generation of Parton Distributions with Uncertainties from Global QCD Analysis”, *Journal of High Energy Physics* **07** (2002) 012, arXiv:hep-ph/0201195 [hep-ex].
- [34] H. Paukkunen, “Nuclear PDFs Today”, *Proceedings of Science HardProbes2018* (2018) 014, arXiv:1811.01976 [hep-ph].
- [35] NNPDF Collaboration, R. D. Ball *et al.*, “Parton distributions from high-precision collider data”, *European Physical Journal C* **77** (2017) 663, arXiv:1706.00428 [hep-ph].
- [36] A. Kusina *et al.*, “Impact of LHC vector boson production in heavy ion collisions on strange PDFs”, *European Physical Journal C* **80** (2020) 968, arXiv:2007.09100 [hep-ph].
- [37] K. J. Eskola, P. Paakkinen, H. Paukkunen, and C. A. Salgado, “EPPS21: A global QCD analysis of nuclear PDFs”, *The European Physical Journal C* **82** (2022) 413, arXiv:2112.12462 [hep-ph].
- [38] ALICE Collaboration, G. Dellacasa *et al.*, “Technical Design Report of the Dimuon Forward Spectrometer”, Tech. Rep. CERN-LHCC-99-022. ALICE-TDR-5, CERN, Aug, 1999. <http://cds.cern.ch/record/401974>.
- [39] ALICE Collaboration, G. Dellacasa *et al.*, “ALICE dimuon forward spectrometer: addendum to the Technical Design Report”, Tech. Rep. CERN-LHCC-2000-046. ALICE-TDR-5-add-1, CERN, Dec, 2000. <http://cds.cern.ch/record/494265>.
- [40] ALICE Collaboration, G. Dellacasa *et al.*, “ALICE Inner Tracking System (ITS): Technical Design Report”, Tech. Rep. CERN-LHCC-99-012. ALICE-TDR-4, CERN, Jun, 1999. <http://cds.cern.ch/record/391175>.
- [41] ALICE Collaboration, P. Cortese *et al.*, “ALICE forward detectors: FMD, T0 and V0: Technical Design Report”, Tech. Rep. CERN-LHCC-2004-025. ALICE-TDR-11, CERN, Sep, 2004. <https://cds.cern.ch/record/781854>.
- [42] S. van der Meer, “Calibration of the effective beam height in the ISR”, Tech. Rep. CERN-ISR-PO-68-31. ISR-PO-68-31, CERN, Geneva, 1968. <https://cds.cern.ch/record/296752>.
- [43] M. Miller, K. Reygers, S. Sanders, and P. Steinberg, “Glauber Modeling in High Energy Nuclear Collisions”, *Annual Review of Nuclear and Particle Science* **57** (2007) 205–243, arXiv:nucl-ex/0701025 [nucl-ex].
- [44] D. d’Enterria and C. Loizides, “Progress in the Glauber Model at Collider Energies”, *Annual Review of Nuclear and Particle Science* **71** (2021) 315–344, arXiv:2011.14909 [hep-ph].
- [45] ALICE Collaboration, J. Adam *et al.*, “Centrality dependence of particle production in p–Pb collisions at $\sqrt{s_{NN}} = 5.02$ TeV”, *Physical Review C* **91** (2015) 064905, arXiv:1412.6828 [nucl-ex].
- [46] ALICE Collaboration, G. Dellacasa *et al.*, “ALICE Zero-Degree Calorimeter (ZDC): Technical Design Report”, Tech. Rep. CERN-LHCC-99-005. ALICE-TDR-3, CERN, Mar, 1999. <https://cds.cern.ch/record/381433>.

- [47] **ALICE** Collaboration, K. Aamodt *et al.*, “The ALICE experiment at the CERN LHC”, *Journal of Instrumentation* **3** (2008) S08002. <http://cds.cern.ch/record/1129812>. Also published by CERN Geneva in 2010.
- [48] **ALICE** Collaboration, B. B. Abelev *et al.*, “Performance of the ALICE Experiment at the CERN LHC”, *International Journal of Modern Physics A* **29** (2014) 1430044, arXiv:1402.4476 [nucl-ex].
- [49] **ALICE** Collaboration, A. Acharya *et al.*, “ALICE luminosity determination for p–Pb collisions at $\sqrt{s_{NN}} = 8.16$ TeV”, Tech. Rep. ALICE-PUBLIC-2018-002, CERN, Apr, 2018. <https://cds.cern.ch/record/2314660>.
- [50] **ALICE** Collaboration, “ALICE luminosity determination for Pb–Pb collisions at $\sqrt{s_{NN}} = 5.02$ TeV”, arXiv:2204.10148 [nucl-ex].
- [51] C. Loizides, J. Kamin, and D. d’Enterria, “Improved Monte Carlo Glauber predictions at present and future nuclear colliders”, *Physical Review C* **97** (2018) 054910, arXiv:1710.07098 [nucl-ex].
- [52] **ALICE** Collaboration, S. Acharya *et al.*, “Centrality determination in heavy ion collisions”, Tech. Rep. ALICE-PUBLIC-2018-011, CERN, Aug, 2018. <https://cds.cern.ch/record/2636623>.
- [53] S. Aioli, P. Nason, C. Oleari, and E. Re, “NLO vector-boson production matched with shower in POWHEG”, *Journal of High Energy Physics* **07** (2008) 060, arXiv:0805.4802 [hep-ph].
- [54] T. Sjostran, S. Mrenna, and P. Skands, “PYTHIA 6.4 physics and manual”, *Journal of High Energy Physics* **05** (2006) 026, arXiv:hep-ph/0603175 [hep-ph].
- [55] H.-L. Lai, M. Guzzi, J. Huston, Z. Li, P. M. Nadolsky, J. Pumplin, and C.-P. Yuan, “New parton distributions for collider physics”, *Physical Review D* **82** (2010) 074024, arXiv:1007.2241 [hep-ph].
- [56] K. J. Eskola, H. Paukkunen, and C. A. Salgado, “EPS09 - a New Generation of NLO and LO Nuclear Parton Distribution Functions”, *Journal of High Energy Physics* **04** (2009) 065, arXiv:0902.4154 [hep-ph].
- [57] M. Cacciari, M. Greco, and P. Nason, “The p(T) spectrum in Heavy-Flavour Hadroproduction”, *Journal of High Energy Physics* **05** (1998) 007, arXiv:hep-ph/9803400 [hep-ph].
- [58] S. Acharya *et al.*, “Production of muons from heavy-flavour hadron decays in p–Pb collisions at $\sqrt{s_{NN}} = 5.02$ TeV”, *Physics Letters B* **770** (2017) 459–472, arXiv:1702.01479 [nucl-ex].
- [59] M. Nahrgang, J. Aichelin, P. B. Gossiaux, and K. Werner, “Influence of hadronic bound states above T_c on heavy-quark observables in Pb + Pb collisions at the CERN Large Hadron Collider”, *Physical Review C* **89** (2014) 014905, arXiv:1305.6544 [hep-ph].
- [60] R. Brun, F. Bruyant, F. Carminati, S. Giani, M. Maire, A. McPherson, G. Patrick, and L. Urban, “GEANT: Detector Description and Simulation Tool”, 1994. <https://cds.cern.ch/record/1082634>. CERN-W-5013.
- [61] V. Blobel and C. Kleinwort, “A New method for the high precision alignment of track detectors”, in *Advanced Statistical Techniques in Particle Physics*. 2002. arXiv:hep-ex/0208021 [hep-ex].


- [62] **ALICE** Collaboration, J. Adam *et al.*, “Quarkonium signal extraction in ALICE”, Tech. Rep. ALICE-PUBLIC-2015-006, CERN, Oct, 2015. <https://cds.cern.ch/record/2060096>.
- [63] K. J. Eskola, V. J. Kolhinen, and C. A. Salgado, “The scale dependent nuclear effects in parton distributions for practical applications”, *European Physical Journal C* **09** (1999) 61–68, [arXiv:hep-ph/9807297](https://arxiv.org/abs/hep-ph/9807297) [hep-ph].
- [64] T. Campbell and T. Neumann, “Precision phenomenology with MCFM”, *Journal of High Energy Physics* **12** (2019) 034, [arXiv:1909.09117](https://arxiv.org/abs/1909.09117) [hep-ph].
- [65] R. Gavin, Y. Li, F. Petriello, and S. Quackenbush, “FEWZ 2.0: A code for hadronic Z production at next-to-next-to-leading order”, *Computer Physics Communications* **182** (2011) 2388–2403, [arXiv:1011.3540](https://arxiv.org/abs/1011.3540) [hep-ph].
- [66] S. Alekhin, A. Kardos, S. Moch, and Z. Trocsanyi, “Precision studies for Drell-Yan processes at NNLO”, *The European Physical Journal C* **81** (2021) 573, [arXiv:2104.02400](https://arxiv.org/abs/2104.02400) [hep-ph].
- [67] S. Dulat, T. J. Hou, J. Gao, M. Guzzi, J. Huston, P. Nadolsky, J. Pumplin, C. Schmidt, D. Stump, and C. P. Yuan, “New parton distribution functions from a global analysis of quantum chromodynamics”, *Physical Review D* **93** (2016) 033006, [arXiv:1506.07443](https://arxiv.org/abs/1506.07443) [hep-ph].
- [68] **LHCb** Collaboration, R. Aaij *et al.*, “Measurement of forward W and Z production in pp collisions at $\sqrt{s} = 8$ TeV”, *Journal of High Energy Physics* **01** (2016) 155, [arXiv:1511.08039](https://arxiv.org/abs/1511.08039) [hep-ex].
- [69] P. M. Nadolsky, H.-L. Lai, Q.-H. Cao, J. Huston, J. Pumplin, D. Stump, W.-K. Tung, and C.-P. Yuan, “Implications of CTEQ global analysis for collider observables”, *Physical Review D* **78** (2008) 013004, [arXiv:0802.0007](https://arxiv.org/abs/0802.0007) [hep-ph].
- [70] V. Emel’yanov, A. Khodinov, S. R. Klein, and R. Vogt, “The Effect of shadowing on initial conditions, transverse energy and hard probes in ultrarelativistic heavy ion collisions”, *Physical Review C* **61** (2000) 044904, [arXiv:hep-ph/9909427](https://arxiv.org/abs/hep-ph/9909427) [hep-ph].
- [71] I. Helenius, K. J. Eskola, H. Honkanen, and C. A. Salgado, “Impact-Parameter Dependent Nuclear Parton Distribution Functions: EPS09s and EKS98s and Their Applications in Nuclear Hard Processes”, *Journal of High Energy Physics* **07** (2012) 073, [arXiv:1205.5359](https://arxiv.org/abs/1205.5359) [hep-ph].
- [72] K. J. Eskola, I. Helenius, M. Kuha, and H. Paukkunen, “Shadowing in inelastic nucleon-nucleon cross section?”, *Physics Review Letters* **125** (2020) 212301, [arXiv:2003.11856](https://arxiv.org/abs/2003.11856) [hep-ph].
- [73] **ALICE** Collaboration, S. Acharya *et al.*, “Analysis of the apparent nuclear modification in peripheral Pb–Pb collisions at 5.02 TeV”, *Physics Letters B* **793** (2019) 420–432, [arXiv:1805.05212](https://arxiv.org/abs/1805.05212) [nucl-ex].
- [74] C. Loizides and A. Morsch, “Absence of jet quenching in peripheral nucleus-nucleus collisions”, *Physics Letters B* **773** (2017) 408–411, [arXiv:1705.08856](https://arxiv.org/abs/1705.08856) [nucl-ex].
- [75] F. Jonas and C. Loizides, “Centrality dependence of electroweak boson production in PbPb collisions at the LHC”, *Physical Review C* **104** (2021) 044905, [arXiv:2104.14903](https://arxiv.org/abs/2104.14903) [nucl-ex].

A The ALICE Collaboration

S. Acharya ^{124,131}, D. Adamová ⁸⁶, A. Adler⁶⁹, G. Aglieri Rinella ³², M. Agnello ²⁹, N. Agrawal ⁵⁰, Z. Ahammed ¹³¹, S. Ahmad ¹⁵, S.U. Ahn ⁷⁰, I. Ahuja ³⁷, A. Akindinov ¹³⁹, M. Al-Turany ⁹⁸, D. Aleksandrov ¹³⁹, B. Alessandro ⁵⁵, H.M. Alfanda ⁶, R. Alfaro Molina ⁶⁶, B. Ali ¹⁵, Y. Ali¹³, A. Alici ²⁵, N. Alizadehvandchali ¹¹³, A. Alkin ³², J. Alme ²⁰, G. Alocco ⁵¹, T. Alt ⁶³, I. Altsybeev ¹³⁹, M.N. Anaam ⁶, C. Andrei ⁴⁵, A. Andronic ¹³⁴, V. Anguelov ⁹⁵, F. Antinori ⁵³, P. Antonioli ⁵⁰, C. Anuj ¹⁵, N. Apadula ⁷⁴, L. Aphecetche ¹⁰³, H. Appelshäuser ⁶³, S. Arcelli ²⁵, R. Arnaldi ⁵⁵, I.C. Arsene ¹⁹, M. Arslanok ¹³⁶, A. Augustinus ³², R. Averbeck ⁹⁸, S. Aziz ⁷², M.D. Azmi ¹⁵, A. Badalà ⁵², Y.W. Baek ⁴⁰, X. Bai ⁹⁸, R. Bailhache ⁶³, Y. Bailung ⁴⁷, R. Bala ⁹¹, A. Balbino ²⁹, A. Baldisseri ¹²⁷, B. Balis ², D. Banerjee ⁴, Z. Banoo ⁹¹, R. Barbera ²⁶, L. Barioglio ⁹⁶, M. Barlou⁷⁸, G.G. Barnaföldi ¹³⁵, L.S. Barnby ⁸⁵, V. Barret ¹²⁴, L. Barreto ¹⁰⁹, C. Bartels ¹¹⁶, K. Barth ³², E. Bartsch ⁶³, F. Baruffaldi ²⁷, N. Bastid ¹²⁴, S. Basu ⁷⁵, G. Batigne ¹⁰³, D. Battistini ⁹⁶, B. Batyunya ¹⁴⁰, D. Bauri⁴⁶, J.L. Bazo Alba ¹⁰¹, I.G. Bearden ⁸³, C. Beattie ¹³⁶, P. Becht ⁹⁸, D. Behera ⁴⁷, I. Belikov ¹²⁶, A.D.C. Bell Hechavarria ¹³⁴, F. Bellini ²⁵, R. Bellwied ¹¹³, S. Belokurova ¹³⁹, V. Belyaev ¹³⁹, G. Bencedi ^{135,64}, S. Beole ²⁴, A. Bercuci ⁴⁵, Y. Berdnikov ¹³⁹, A. Berdnikova ⁹⁵, L. Bergmann ⁹⁵, M.G. Besoiu ⁶², L. Betev ³², P.P. Bhaduri ¹³¹, A. Bhasin ⁹¹, I.R. Bhat⁹¹, M.A. Bhat ⁴, B. Bhattacharjee ⁴¹, L. Bianchi ²⁴, N. Bianchi ⁴⁸, J. Bielčik ³⁵, J. Bielčíková ⁸⁶, J. Biernat ¹⁰⁶, A. Bilandzic ⁹⁶, G. Biro ¹³⁵, S. Biswas ⁴, J.T. Blair ¹⁰⁷, D. Blau ¹³⁹, M.B. Blidaru ⁹⁸, N. Bluhme³⁸, C. Blume ⁶³, G. Boca ^{21,54}, F. Bock ⁸⁷, T. Bodova ²⁰, A. Bogdanov¹³⁹, S. Boi ²², J. Bok ⁵⁷, L. Boldizsár ¹³⁵, A. Bolozdynya ¹³⁹, M. Bombara ³⁷, P.M. Bond ³², G. Bonomi ^{130,54}, H. Borel ¹²⁷, A. Borissov ¹³⁹, H. Bossi ¹³⁶, E. Botta ²⁴, L. Bratrud ⁶³, P. Braun-Munzinger ⁹⁸, M. Bregant ¹⁰⁹, M. Broz ³⁵, G.E. Bruno ^{97,31}, M.D. Buckland ¹¹⁶, D. Budnikov ¹³⁹, H. Buesching ⁶³, S. Bufalino ²⁹, O. Bugnon¹⁰³, P. Buhler ¹⁰², Z. Buthelezi ^{67,120}, J.B. Butt¹³, A. Bylinkin ¹¹⁵, S.A. Bysiak¹⁰⁶, M. Cai ^{27,6}, H. Caines ¹³⁶, A. Caliva ⁹⁸, E. Calvo Villar ¹⁰¹, J.M.M. Camacho ¹⁰⁸, R.S. Camacho⁴⁴, P. Camerini ²³, F.D.M. Canedo ¹⁰⁹, M. Carabas ¹²³, F. Carnesecchi ³², R. Caron ^{125,127}, J. Castillo Castellanos ¹²⁷, F. Catalano ²⁹, C. Ceballos Sanchez ¹⁴⁰, I. Chakaberia ⁷⁴, P. Chakraborty ⁴⁶, S. Chandra ¹³¹, S. Chapeland ³², M. Chartier ¹¹⁶, S. Chattopadhyay ¹³¹, S. Chattopadhyay ⁹⁹, T.G. Chavez ⁴⁴, T. Cheng ⁶, C. Cheshkov ¹²⁵, B. Cheynis ¹²⁵, V. Chibante Barroso ³², D.D. Chinellato ¹¹⁰, E.S. Chizzali ^{11,96}, J. Cho ⁵⁷, S. Cho ⁵⁷, P. Chochula ³², P. Christakoglou ⁸⁴, C.H. Christensen ⁸³, P. Christiansen ⁷⁵, T. Chujo ¹²², M. Ciaccio ²⁹, C. Cicalo ⁵¹, L. Cifarelli ²⁵, F. Cindolo ⁵⁰, M.R. Ciupek⁹⁸, G. Clai^{III,50}, F. Colamaria ⁴⁹, J.S. Colburn¹⁰⁰, D. Colella ^{97,31}, A. Collu⁷⁴, M. Colocci ³², M. Concas ^{IV,55}, G. Conesa Balbastre ⁷³, Z. Conesa del Valle ⁷², G. Contin ²³, J.G. Contreras ³⁵, M.L. Coquet ¹²⁷, T.M. Cormier^{I,87}, P. Cortese ^{129,55}, M.R. Cosentino ¹¹¹, F. Costa ³², S. Costanza ^{21,54}, P. Crochet ¹²⁴, R. Cruz-Torres ⁷⁴, E. Cuautle⁶⁴, P. Cui ⁶, L. Cunqueiro⁸⁷, A. Dainese ⁵³, M.C. Danisch ⁹⁵, A. Danu ⁶², P. Das ⁸⁰, P. Das ⁴, S. Das ⁴, S. Dash ⁴⁶, A. De Caro ²⁸, G. de Cataldo ⁴⁹, L. De Cilladi ²⁴, J. de Cuveland³⁸, A. De Falco ²², D. De Gruttola ²⁸, N. De Marco ⁵⁵, C. De Martin ²³, S. De Pasquale ²⁸, S. Deb ⁴⁷, H.F. Degenhardt¹⁰⁹, K.R. Deja¹³², R. Del Grande ⁹⁶, L. Dello Stritto ²⁸, W. Deng ⁶, P. Dhankher ¹⁸, D. Di Bari ³¹, A. Di Mauro ³², R.A. Diaz ^{140,7}, T. Dietel ¹¹², Y. Ding ^{125,6}, R. Divià ³², D.U. Dixit ¹⁸, Ø. Djuvsland²⁰, U. Dmitrieva ¹³⁹, A. Dobrin ⁶², B. Dönigus ⁶³, A.K. Dubey ¹³¹, J.M. Dubinski¹³², A. Dubla ⁹⁸, S. Dudi ⁹⁰, P. Dupieux ¹²⁴, M. Durkac¹⁰⁵, N. Dzalaiova¹², T.M. Eder ¹³⁴, R.J. Ehlers ⁸⁷, V.N. Eikeland²⁰, F. Eisenhut ⁶³, D. Elia ⁴⁹, B. Erazmus ¹⁰³, F. Ercolessi ²⁵, F. Erhardt ⁸⁹, M.R. Erstad²⁰, B. Espagnon ⁷², G. Eulisse ³², D. Evans ¹⁰⁰, S. Evdokimov ¹³⁹, L. Fabbietti ⁹⁶, M. Faggin ²⁷, J. Faivre ⁷³, F. Fan ⁶, W. Fan ⁷⁴, A. Fantoni ⁴⁸, M. Fasel ⁸⁷, P. Fedchio²⁹, A. Feliciello ⁵⁵, G. Feofilov ¹³⁹, A. Fernández Téllez ⁴⁴, M.B. Ferrer ³², A. Ferrero ¹²⁷, A. Ferretti ²⁴, V.J.G. Feuillard ⁹⁵, J. Figiel ¹⁰⁶, V. Filova³⁵, D. Finogeev ¹³⁹, F.M. Fionda ⁵¹, G. Fiorenza⁹⁷, F. Flor ¹¹³, A.N. Flores ¹⁰⁷, S. Foertsch ⁶⁷, I. Fokin ⁹⁵, S. Fokin ¹³⁹, E. Fragiaco ⁵⁶, E. Frajna ¹³⁵, U. Fuchs ³², N. Funicello ²⁸, C. Furget ⁷³, A. Furs ¹³⁹, J.J. Gaardhøje ⁸³, M. Gagliardi ²⁴, A.M. Gago ¹⁰¹, A. Gal¹²⁶, C.D. Galvan ¹⁰⁸, P. Ganoti ⁷⁸, C. Garabatos ⁹⁸, J.R.A. Garcia ⁴⁴, E. Garcia-Solis ⁹, K. Garg ¹⁰³, C. Gargiulo ³², A. Garibli⁸¹, K. Garner¹³⁴, E.F. Gauger ¹⁰⁷, A. Gautam ¹¹⁵, M.B. Gay Ducati ⁶⁵, M. Germain ¹⁰³, S.K. Ghosh⁴, M. Giacalone ²⁵, P. Gianotti ⁴⁸, P. Giubellino ^{98,55}, P. Giubilato ²⁷, A.M.C. Glaenger ¹²⁷, P. Glässel ⁹⁵, E. Glimos¹¹⁹, D.J.Q. Goh⁷⁶, V. Gonzalez ¹³³, L.H. González-Trueba ⁶⁶, S. Gorbunov³⁸, M. Gorgon ², L. Görlich ¹⁰⁶, S. Gotovac³³, V. Grabski ⁶⁶, L.K. Graczykowski ¹³², E. Grecka ⁸⁶, L. Greiner ⁷⁴, A. Grelli ⁵⁸, C. Grigoras ³², V. Grigoriev ¹³⁹, S. Grigoryan ^{140,1}, F. Grosa ³², J.F. Grosse-Oetringhaus ³², R. Grosso ⁹⁸, D. Grund ³⁵, G.G. Guardiano ¹¹⁰, R. Guernane ⁷³, M. Guilbaud ¹⁰³, K. Gulbrandsen ⁸³, T. Gunji ¹²¹,

W. Guo⁶, A. Gupta⁹¹, R. Gupta⁹¹, S.P. Guzman⁴⁴, L. Gyulai¹³⁵, M.K. Habib⁹⁸, C. Hadjidakis⁷², H. Hamagaki⁷⁶, M. Hamid⁶, Y. Han¹³⁷, R. Hannigan¹⁰⁷, M.R. Haque¹³², A. Harlenderova⁹⁸, J.W. Harris¹³⁶, A. Harton⁹, J.A. Hasenbichler³², H. Hassan⁸⁷, D. Hatzifotiadou⁵⁰, P. Hauer⁴², L.B. Havener¹³⁶, S.T. Heckel⁹⁶, E. Hellbär⁹⁸, H. Helstrup³⁴, T. Herman³⁵, G. Herrera Corral⁸, F. Herrmann¹³⁴, K.F. Hetland³⁴, B. Heybeck⁶³, H. Hillemanns³², C. Hills¹¹⁶, B. Hippolyte¹²⁶, B. Hofman⁵⁸, B. Hohlweger⁸⁴, J. Honermann¹³⁴, G.H. Hong¹³⁷, D. Horak³⁵, A. Horzyk², R. Hosokawa¹⁴, Y. Hou⁶, P. Hristov³², C. Hughes¹¹⁹, P. Huhn⁶³, L.M. Huhta¹¹⁴, C.V. Hulse⁷², T.J. Humanic⁸⁸, H. Hushnud⁹⁹, A. Hutson¹¹³, D. Hutter³⁸, J.P. Iddon¹¹⁶, R. Ilkaev¹³⁹, H. Ilyas¹³, M. Inaba¹²², G.M. Innocenti³², M. Ippolitov¹³⁹, A. Isakov⁸⁶, T. Isidori¹¹⁵, M.S. Islam⁹⁹, M. Ivanov⁹⁸, V. Ivanov¹³⁹, V. Izucheev¹³⁹, M. Jablonski², B. Jacak⁷⁴, N. Jacazio³², P.M. Jacobs⁷⁴, S. Jadlovská¹⁰⁵, J. Jadlovsky¹⁰⁵, L. Jaffe³⁸, C. Jahnke¹¹⁰, M.A. Janik¹³², T. Janson⁶⁹, M. Jercic⁸⁹, O. Jevons¹⁰⁰, A.A.P. Jimenez⁶⁴, F. Jonas^{87,134}, P.G. Jones¹⁰⁰, J.M. Jowett^{32,98}, J. Jung⁶³, M. Jung⁶³, A. Junique³², A. Jusko¹⁰⁰, M.J. Kabus^{32,132}, J. Kaewjai¹⁰⁴, P. Kalinak⁵⁹, A.S. Kalteyer⁹⁸, A. Kalweit³², V. Kaplin¹³⁹, A. Karasu Uysal⁷¹, D. Karatovic⁸⁹, O. Karavichev¹³⁹, T. Karavicheva¹³⁹, P. Karczmarczyk¹³², E. Karpechev¹³⁹, V. Kashyap⁸⁰, A. Kazantsev¹³⁹, U. Keschull⁶⁹, R. Keidel¹³⁸, D.L.D. Keijdener⁵⁸, M. Keil³², B. Ketzer⁴², A.M. Khan⁶, S. Khan¹⁵, A. Khanzadeev¹³⁹, Y. Kharlov¹³⁹, A. Khatun¹⁵, A. Khuntia¹⁰⁶, B. Kileng³⁴, B. Kim¹⁶, C. Kim¹⁶, D.J. Kim¹¹⁴, E.J. Kim⁶⁸, J. Kim¹³⁷, J.S. Kim⁴⁰, J. Kim⁹⁵, J. Kim⁶⁸, M. Kim⁹⁵, S. Kim¹⁷, T. Kim¹³⁷, S. Kirsch⁶³, I. Kisel³⁸, S. Kiselev¹³⁹, A. Kisiel¹³², J.P. Kitowski², J.L. Klay⁵, J. Klein³², S. Klein⁷⁴, C. Klein-Bösing¹³⁴, M. Kleiner⁶³, T. Klemenz⁹⁶, A. Kluge³², A.G. Knospe¹¹³, C. Kobdaj¹⁰⁴, T. Kollegger⁹⁸, A. Kondratyev¹⁴⁰, N. Kondratyeva¹³⁹, E. Kondratyuk¹³⁹, J. Konig⁶³, S.A. Konigstorfer⁹⁶, P.J. Konopka³², G. Kornakov¹³², S.D. Koryciak², A. Kotliarov⁸⁶, O. Kovalenko⁷⁹, V. Kovalenko¹³⁹, M. Kowalski¹⁰⁶, I. Králik⁵⁹, A. Kravčáková³⁷, L. Kreis⁹⁸, M. Krivda^{100,59}, F. Krizek⁸⁶, K. Krizkova Gajdosova³⁵, M. Kroesen⁹⁵, M. Krüger⁶³, D.M. Krupova³⁵, E. Kryshen¹³⁹, M. Krzewicki³⁸, V. Kučera³², C. Kuhn¹²⁶, P.G. Kuijjer⁸⁴, T. Kumaoka¹²², D. Kumar¹³¹, L. Kumar⁹⁰, N. Kumar⁹⁰, S. Kundu³², P. Kurashvili⁷⁹, A. Kurepin¹³⁹, A.B. Kurepin¹³⁹, S. Kushpil⁸⁶, J. Kvapil¹⁰⁰, M.J. Kwon⁵⁷, J.Y. Kwon⁵⁷, Y. Kwon¹³⁷, S.L. La Pointe³⁸, P. La Rocca²⁶, Y.S. Lai⁷⁴, A. Lakrathok¹⁰⁴, M. Lamanna³², R. Langoy¹¹⁸, P. Larionov⁴⁸, E. Laudi³², L. Lautner^{32,96}, R. Lavicka¹⁰², T. Lazareva¹³⁹, R. Lea^{130,54}, J. Lehrbach³⁸, R.C. Lemmon⁸⁵, I. León Monzón¹⁰⁸, M.M. Lesch⁹⁶, E.D. Lesser¹⁸, M. Lettrich⁹⁶, P. Lévai¹³⁵, X. Li¹⁰, X.L. Li⁶, J. Lien¹¹⁸, R. Lietava¹⁰⁰, B. Lim¹⁶, S.H. Lim¹⁶, V. Lindenstruth³⁸, A. Lindner⁴⁵, C. Lippmann⁹⁸, A. Liu¹⁸, D.H. Liu⁶, J. Liu¹¹⁶, I.M. Lofnes²⁰, V. Loginov¹³⁹, C. Loizides⁸⁷, P. Loncar³³, J.A. Lopez⁹⁵, X. Lopez¹²⁴, E. López Torres⁷, P. Lu^{98,117}, J.R. Luhder¹³⁴, M. Lunardon²⁷, G. Luparello⁵⁶, Y.G. Ma³⁹, A. Maevskaya¹³⁹, M. Mager³², T. Mahmoud⁴², A. Maire¹²⁶, M. Malaev¹³⁹, N.M. Malik⁹¹, Q.W. Malik¹⁹, S.K. Malik⁹¹, L. Malinina^{VII,140}, D. Mal'Kevich¹³⁹, D. Mallick⁸⁰, N. Mallick⁴⁷, G. Mandaglio^{30,52}, V. Manko¹³⁹, F. Manso¹²⁴, V. Manzari⁴⁹, Y. Mao⁶, G.V. Margagliotti²³, A. Margotti⁵⁰, A. Marín⁹⁸, C. Markert¹⁰⁷, M. Marquard⁶³, N.A. Martin⁹⁵, P. Martinengo³², J.L. Martinez¹¹³, M.I. Martínez⁴⁴, G. Martínez García¹⁰³, S. Masciocchi⁹⁸, M. Maserà²⁴, A. Masoni⁵¹, L. Massacrier⁷², A. Mastroserio^{128,49}, A.M. Mathis⁹⁶, O. Matonoha⁷⁵, P.F.T. Matuoka¹⁰⁹, A. Matyja¹⁰⁶, C. Mayer¹⁰⁶, A.L. Mazuecos³², F. Mazzaschi²⁴, M. Mazzilli³², J.E. Mdhuli¹²⁰, A.F. Mechler⁶³, Y. Melikyan¹³⁹, A. Menchaca-Rocha⁶⁶, E. Meninno^{102,28}, A.S. Menon¹¹³, M. Meres¹², S. Mhlanga^{112,67}, Y. Miake¹²², L. Micheletti⁵⁵, L.C. Migliorin¹²⁵, D.L. Mihaylov⁹⁶, K. Mikhaylov^{140,139}, A.N. Mishra¹³⁵, D. Miśkowiec⁹⁸, A. Modak⁴, A.P. Mohanty⁵⁸, B. Mohanty⁸⁰, M. Mohisin Khan^{V,15}, M.A. Molander⁴³, Z. Moravcova⁸³, C. Mordasini⁹⁶, D.A. Moreira De Godoy¹³⁴, I. Morozov¹³⁹, A. Morsch³², T. Mrnjavac³², V. Muccifora⁴⁸, E. Mudnic³³, S. Muhuri¹³¹, J.D. Mulligan⁷⁴, A. Mulliri²², M.G. Munhoz¹⁰⁹, R.H. Munzer⁶³, H. Murakami¹²¹, S. Murray¹¹², L. Musa³², J. Musinsky⁵⁹, J.W. Myrcha¹³², B. Naik¹²⁰, R. Nair⁷⁹, B.K. Nandi⁴⁶, R. Nania⁵⁰, E. Nappi⁴⁹, A.F. Nassirpour⁷⁵, A. Nath⁹⁵, C. Natrass¹¹⁹, A. Neagu¹⁹, A. Negru¹²³, L. Nellen⁶⁴, S.V. Nesbo³⁴, G. Neskovic³⁸, D. Nesterov¹³⁹, B.S. Nielsen⁸³, E.G. Nielsen⁸³, S. Nikolaev¹³⁹, S. Nikulin¹³⁹, V. Nikulin¹³⁹, F. Noferini⁵⁰, S. Noh¹¹, P. Nomokonov¹⁴⁰, J. Norman¹¹⁶, N. Novitzky¹²², P. Nowakowski¹³², A. Nyanin¹³⁹, J. Nystrand²⁰, M. Ogino⁷⁶, A. Ohlson⁷⁵, V.A. Okorokov¹³⁹, J. Olińczak¹³², A.C. Oliveira Da Silva¹¹⁹, M.H. Oliver¹³⁶, A. Onnerstad¹¹⁴, C. Oppedisano⁵⁵, A. Ortiz Velasquez⁶⁴, A. Oskarsson⁷⁵, J. Otwinowski¹⁰⁶, M. Oya⁹³, K. Oyama⁷⁶, Y. Pachmayer⁹⁵, S. Padhan⁴⁶, D. Pagano^{130,54}, G. Paic⁶⁴, A. Palasciano⁴⁹, S. Panebianco¹²⁷, J. Park⁵⁷, J.E. Parkkila^{32,114}, S.P. Pathak¹¹³, R.N. Patra⁹¹, B. Paul²², H. Pei⁶, T. Peitzmann⁵⁸, X. Peng⁶,

L.G. Pereira ⁶⁵, H. Pereira Da Costa ¹²⁷, D. Peresunko ¹³⁹, G.M. Perez ⁷, S. Perrin ¹²⁷, Y. Pestov ¹³⁹, V. Petráček ³⁵, V. Petrov ¹³⁹, M. Petrovici ⁴⁵, R.P. Pezzi ^{103,65}, S. Piano ⁵⁶, M. Pikna ¹², P. Pillot ¹⁰³, O. Pinazza ^{50,32}, L. Pinsky ¹¹³, C. Pinto ^{96,26}, S. Pisano ⁴⁸, M. Płoskoń ⁷⁴, M. Planinic ⁸⁹, F. Pliquet ⁶³, M.G. Poghosyan ⁸⁷, S. Politano ²⁹, N. Poljak ⁸⁹, A. Pop ⁴⁵, S. Porteboeuf-Houssais ¹²⁴, J. Porter ⁷⁴, V. Pozdniakov ¹⁴⁰, S.K. Prasad ⁴, S. Prasad ⁴⁷, R. Preghenella ⁵⁰, F. Prino ⁵⁵, C.A. Pruneau ¹³³, I. Pshenichnov ¹³⁹, M. Puccio ³², S. Qiu ⁸⁴, L. Quaglia ²⁴, R.E. Quishpe ¹¹³, S. Ragoni ¹⁰⁰, A. Rakotozafindrabe ¹²⁷, L. Ramello ^{129,55}, F. Rami ¹²⁶, S.A.R. Ramirez ⁴⁴, T.A. Rancien ⁷³, R. Raniwala ⁹², S. Raniwala ⁹², S.S. Räsänen ⁴³, R. Rath ⁴⁷, I. Ravasenga ⁸⁴, K.F. Read ^{87,119}, A.R. Redelbach ³⁸, K. Redlich ^{VI,79}, A. Rehman ²⁰, P. Reichelt ⁶³, F. Reidt ³², H.A. Reme-Ness ³⁴, Z. Rescakova ³⁷, K. Reygers ⁹⁵, A. Riabov ¹³⁹, V. Riabov ¹³⁹, R. Ricci ²⁸, T. Richert ⁷⁵, M. Richter ¹⁹, W. Riegler ³², F. Riggi ²⁶, C. Ristea ⁶², M. Rodríguez Cahuantzi ⁴⁴, K. Røed ¹⁹, R. Rogalev ¹³⁹, E. Rogochaya ¹⁴⁰, T.S. Rogoschinski ⁶³, D. Rohr ³², D. Röhrich ²⁰, P.F. Rojas ⁴⁴, S. Rojas Torres ³⁵, P.S. Rokita ¹³², F. Ronchetti ⁴⁸, A. Rosano ^{30,52}, E.D. Rosas ⁶⁴, A. Rossi ⁵³, A. Roy ⁴⁷, P. Roy ⁹⁹, S. Roy ⁴⁶, N. Rubini ²⁵, O.V. Rueda ⁷⁵, D. Ruggiano ¹³², R. Rui ²³, B. Rumyantsev ¹⁴⁰, P.G. Russek ², R. Russo ⁸⁴, A. Rustamov ⁸¹, E. Ryabinkin ¹³⁹, Y. Ryabov ¹³⁹, A. Rybicki ¹⁰⁶, H. Rytkonen ¹¹⁴, W. Rzesza ¹³², O.A.M. Saarimaki ⁴³, R. Sadek ¹⁰³, S. Sadovsky ¹³⁹, J. Saetre ²⁰, K. Šafařík ³⁵, S.K. Saha ¹³¹, S. Saha ⁸⁰, B. Sahoo ⁴⁶, P. Sahoo ⁴⁶, R. Sahoo ⁴⁷, S. Sahoo ⁶⁰, D. Sahu ⁴⁷, P.K. Sahu ⁶⁰, J. Saini ¹³¹, K. Sajdakova ³⁷, S. Sakai ¹²², M.P. Salvan ⁹⁸, S. Sambyal ⁹¹, T.B. Saramela ¹⁰⁹, D. Sarkar ¹³³, N. Sarkar ¹³¹, P. Sarma ⁴¹, V. Sarritzu ²², V.M. Sarti ⁹⁶, M.H.P. Sas ¹³⁶, J. Schambach ⁸⁷, H.S. Scheid ⁶³, C. Schiaua ⁴⁵, R. Schicker ⁹⁵, A. Schmah ⁹⁵, C. Schmidt ⁹⁸, H.R. Schmidt ⁹⁴, M.O. Schmidt ³², M. Schmidt ⁹⁴, N.V. Schmidt ^{87,63}, A.R. Schmier ¹¹⁹, R. Schotter ¹²⁶, J. Schukraft ³², K. Schwarz ⁹⁸, K. Schweda ⁹⁸, G. Scioli ²⁵, E. Scomparin ⁵⁵, J.E. Seger ¹⁴, Y. Sekiguchi ¹²¹, D. Sekihata ¹²¹, I. Selyuzhenkov ^{98,139}, S. Senyukov ¹²⁶, J.J. Seo ⁵⁷, D. Serebryakov ¹³⁹, L. Šerkšnytė ⁹⁶, A. Sevcenco ⁶², T.J. Shaba ⁶⁷, A. Shabanov ¹³⁹, A. Shabetai ¹⁰³, R. Shahoyan ³², W. Shaikh ⁹⁹, A. Shangaraev ¹³⁹, A. Sharma ⁹⁰, D. Sharma ⁴⁶, H. Sharma ¹⁰⁶, M. Sharma ⁹¹, N. Sharma ⁹⁰, S. Sharma ⁹¹, U. Sharma ⁹¹, A. Shatat ⁷², O. Sheibani ¹¹³, K. Shigaki ⁹³, M. Shimomura ⁷⁷, S. Shirinkin ¹³⁹, Q. Shou ³⁹, Y. Sibiriak ¹³⁹, S. Siddhanta ⁵¹, T. Siemiarczuk ⁷⁹, T.F. Silva ¹⁰⁹, D. Silvermyr ⁷⁵, T. Simantathammakul ¹⁰⁴, R. Simeonov ³⁶, G. Simonetti ³², B. Singh ⁹¹, B. Singh ⁹⁶, R. Singh ⁸⁰, R. Singh ⁹¹, R. Singh ⁴⁷, V.K. Singh ¹³¹, V. Singhal ¹³¹, T. Sinha ⁹⁹, B. Sitar ¹², M. Sitta ^{129,55}, T.B. Skaali ¹⁹, G. Skorodumovs ⁹⁵, M. Slupecki ⁴³, N. Smirnov ¹³⁶, R.J.M. Snellings ⁵⁸, E.H. Solheim ¹⁹, C. Soncco ¹⁰¹, J. Song ¹¹³, A. Songmoolnak ¹⁰⁴, F. Soramel ²⁷, S. Sorensen ¹¹⁹, R. Spijkers ⁸⁴, I. Sputowska ¹⁰⁶, J. Staa ⁷⁵, J. Stachel ⁹⁵, I. Stan ⁶², P.J. Steffanic ¹¹⁹, S.F. Stiefelmaier ⁹⁵, D. Stocco ¹⁰³, I. Storehaug ¹⁹, M.M. Storetvedt ³⁴, P. Stratmann ¹³⁴, S. Strazzi ²⁵, C.P. Stylianidis ⁸⁴, A.A.P. Suaide ¹⁰⁹, C. Suire ⁷², M. Sukhanov ¹³⁹, M. Suljic ³², V. Sumberia ⁹¹, S. Sumowidagdo ⁸², S. Swain ⁶⁰, A. Szabo ¹², I. Szarka ¹², U. Tabassam ¹³, S.F. Taghavi ⁹⁶, G. TAILLEPIED ^{98,124}, J. Takahashi ¹¹⁰, G.J. Tambave ²⁰, S. Tang ^{124,6}, Z. Tang ¹¹⁷, J.D. Tapia Takaki ¹¹⁵, N. Tapus ¹²³, L.A. Tarasovicova ¹³⁴, M.G. Tarzila ⁴⁵, A. Tauro ³², A. Telesca ³², L. Terlizzi ²⁴, C. Terrevoli ¹¹³, G. Tersimonov ³, S. Thakur ¹³¹, D. Thomas ¹⁰⁷, R. Tieulent ¹²⁵, A. Tikhonov ¹³⁹, A.R. Timmins ¹¹³, M. Tkacik ¹⁰⁵, T. Tkacik ¹⁰⁵, A. Toia ⁶³, N. Topilskaya ¹³⁹, M. Toppi ⁴⁸, F. Torres-Acosta ¹⁸, T. Tork ⁷², A.G. Torres Ramos ³¹, A. Trifiró ^{30,52}, A.S. Triolo ^{30,52}, S. Tripathy ⁵⁰, T. Tripathy ⁴⁶, S. Trogolo ³², V. Trubnikov ³, W.H. Trzaska ¹¹⁴, T.P. Trzcinski ¹³², R. Turrisi ⁵³, T.S. Tveter ¹⁹, K. Ullaland ²⁰, B. Ulukutlu ⁹⁶, A. Uras ¹²⁵, M. Urioni ^{54,130}, G.L. Usai ²², M. Vala ³⁷, N. Valle ²¹, S. Vallero ⁵⁵, L.V.R. van Doremalen ⁵⁸, M. van Leeuwen ⁸⁴, C.A. van Veen ⁹⁵, R.J.G. van Weelden ⁸⁴, P. Vande Vyvre ³², D. Varga ¹³⁵, Z. Varga ¹³⁵, M. Varga-Kofarago ¹³⁵, M. Vasileiou ⁷⁸, A. Vasiliev ¹³⁹, O. Vázquez Doce ⁹⁶, V. Vechernin ¹³⁹, E. Vercellin ²⁴, S. Vergara Limón ⁴⁴, L. Vermunt ⁵⁸, R. Vértesi ¹³⁵, M. Verweij ⁵⁸, L. Vickovic ³³, Z. Vilakazi ¹²⁰, O. Villalobos Baillie ¹⁰⁰, G. VINO ⁴⁹, A. Vinogradov ¹³⁹, T. Virgili ²⁸, V. Vislavicius ⁸³, A. Vodopyanov ¹⁴⁰, B. Volkel ³², M.A. Völkl ⁹⁵, K. Voloshin ¹³⁹, S.A. Voloshin ¹³³, G. Volpe ³¹, B. von Haller ³², I. Vorobyev ⁹⁶, N. Vozniuk ¹³⁹, J. Vrláková ³⁷, B. Wagner ²⁰, C. Wang ³⁹, D. Wang ³⁹, M. Weber ¹⁰², A. Wegrzynek ³², F.T. Weiglhofer ³⁸, S.C. Wenzel ³², J.P. Wessels ¹³⁴, S.L. Weyhmler ¹³⁶, J. Wiechula ⁶³, J. Wikne ¹⁹, G. Wilk ⁷⁹, J. Wilkinson ⁹⁸, G.A. Willems ¹³⁴, B. Windelband ⁹⁵, M. Winn ¹²⁷, J.R. Wright ¹⁰⁷, W. Wu ³⁹, Y. Wu ¹¹⁷, R. Xu ⁶, A.K. Yadav ¹³¹, S. Yalcin ⁷¹, Y. Yamaguchi ⁹³, K. Yamakawa ⁹³, S. Yang ²⁰, S. Yano ⁹³, Z. Yin ⁶, I.-K. Yoo ¹⁶, J.H. Yoon ⁵⁷, S. Yuan ²⁰, A. Yuncu ⁹⁵, V. Zaccolo ²³, C. Zampolli ³², H.J.C. Zanoli ⁵⁸, F. Zanone ⁹⁵, N. Zardoshti ^{32,100}, A. Zarochentsev ¹³⁹, P. Závada ⁶¹, N. Zaviyalov ¹³⁹, M. Zhalov ¹³⁹, B. Zhang ⁶, S. Zhang ³⁹, X. Zhang ⁶, Y. Zhang ¹¹⁷, M. Zhao ¹⁰, V. Zherebchevskii ¹³⁹, Y. Zhi ¹⁰, N. Zhigareva ¹³⁹, D. Zhou ⁶, Y. Zhou ⁸³, J. Zhu ^{98,6}, Y. Zhu ⁶,

G. Zinovjev^{1,3}, N. Zurlo ^{130,54}

Affiliation Notes

^I Deceased^{II} Also at: Max-Planck-Institut für Physik, Munich, Germany^{III} Also at: Italian National Agency for New Technologies, Energy and Sustainable Economic Development (ENEA), Bologna, Italy^{IV} Also at: Dipartimento DET del Politecnico di Torino, Turin, Italy^V Also at: Department of Applied Physics, Aligarh Muslim University, Aligarh, India^{VI} Also at: Institute of Theoretical Physics, University of Wrocław, Poland^{VII} Also at: An institution covered by a cooperation agreement with CERN

Collaboration Institutes

¹ A.I. Alikhanyan National Science Laboratory (Yerevan Physics Institute) Foundation, Yerevan, Armenia² AGH University of Science and Technology, Cracow, Poland³ Bogolyubov Institute for Theoretical Physics, National Academy of Sciences of Ukraine, Kiev, Ukraine⁴ Bose Institute, Department of Physics and Centre for Astroparticle Physics and Space Science (CAPSS), Kolkata, India⁵ California Polytechnic State University, San Luis Obispo, California, United States⁶ Central China Normal University, Wuhan, China⁷ Centro de Aplicaciones Tecnológicas y Desarrollo Nuclear (CEADEN), Havana, Cuba⁸ Centro de Investigación y de Estudios Avanzados (CINVESTAV), Mexico City and Mérida, Mexico⁹ Chicago State University, Chicago, Illinois, United States¹⁰ China Institute of Atomic Energy, Beijing, China¹¹ Chungbuk National University, Cheongju, Republic of Korea¹² Comenius University Bratislava, Faculty of Mathematics, Physics and Informatics, Bratislava, Slovak Republic¹³ COMSATS University Islamabad, Islamabad, Pakistan¹⁴ Creighton University, Omaha, Nebraska, United States¹⁵ Department of Physics, Aligarh Muslim University, Aligarh, India¹⁶ Department of Physics, Pusan National University, Pusan, Republic of Korea¹⁷ Department of Physics, Sejong University, Seoul, Republic of Korea¹⁸ Department of Physics, University of California, Berkeley, California, United States¹⁹ Department of Physics, University of Oslo, Oslo, Norway²⁰ Department of Physics and Technology, University of Bergen, Bergen, Norway²¹ Dipartimento di Fisica, Università di Pavia, Pavia, Italy²² Dipartimento di Fisica dell'Università and Sezione INFN, Cagliari, Italy²³ Dipartimento di Fisica dell'Università and Sezione INFN, Trieste, Italy²⁴ Dipartimento di Fisica dell'Università and Sezione INFN, Turin, Italy²⁵ Dipartimento di Fisica e Astronomia dell'Università and Sezione INFN, Bologna, Italy²⁶ Dipartimento di Fisica e Astronomia dell'Università and Sezione INFN, Catania, Italy²⁷ Dipartimento di Fisica e Astronomia dell'Università and Sezione INFN, Padova, Italy²⁸ Dipartimento di Fisica 'E.R. Caianiello' dell'Università and Gruppo Collegato INFN, Salerno, Italy²⁹ Dipartimento DISAT del Politecnico and Sezione INFN, Turin, Italy³⁰ Dipartimento di Scienze MIFT, Università di Messina, Messina, Italy³¹ Dipartimento Interateneo di Fisica 'M. Merlin' and Sezione INFN, Bari, Italy³² European Organization for Nuclear Research (CERN), Geneva, Switzerland³³ Faculty of Electrical Engineering, Mechanical Engineering and Naval Architecture, University of Split, Split, Croatia³⁴ Faculty of Engineering and Science, Western Norway University of Applied Sciences, Bergen, Norway³⁵ Faculty of Nuclear Sciences and Physical Engineering, Czech Technical University in Prague, Prague, Czech Republic³⁶ Faculty of Physics, Sofia University, Sofia, Bulgaria³⁷ Faculty of Science, P.J. Šafárik University, Košice, Slovak Republic³⁸ Frankfurt Institute for Advanced Studies, Johann Wolfgang Goethe-Universität Frankfurt, Frankfurt, Germany

- ³⁹ Fudan University, Shanghai, China
- ⁴⁰ Gangneung-Wonju National University, Gangneung, Republic of Korea
- ⁴¹ Gauhati University, Department of Physics, Guwahati, India
- ⁴² Helmholtz-Institut für Strahlen- und Kernphysik, Rheinische Friedrich-Wilhelms-Universität Bonn, Bonn, Germany
- ⁴³ Helsinki Institute of Physics (HIP), Helsinki, Finland
- ⁴⁴ High Energy Physics Group, Universidad Autónoma de Puebla, Puebla, Mexico
- ⁴⁵ Horia Hulubei National Institute of Physics and Nuclear Engineering, Bucharest, Romania
- ⁴⁶ Indian Institute of Technology Bombay (IIT), Mumbai, India
- ⁴⁷ Indian Institute of Technology Indore, Indore, India
- ⁴⁸ INFN, Laboratori Nazionali di Frascati, Frascati, Italy
- ⁴⁹ INFN, Sezione di Bari, Bari, Italy
- ⁵⁰ INFN, Sezione di Bologna, Bologna, Italy
- ⁵¹ INFN, Sezione di Cagliari, Cagliari, Italy
- ⁵² INFN, Sezione di Catania, Catania, Italy
- ⁵³ INFN, Sezione di Padova, Padova, Italy
- ⁵⁴ INFN, Sezione di Pavia, Pavia, Italy
- ⁵⁵ INFN, Sezione di Torino, Turin, Italy
- ⁵⁶ INFN, Sezione di Trieste, Trieste, Italy
- ⁵⁷ Inha University, Incheon, Republic of Korea
- ⁵⁸ Institute for Gravitational and Subatomic Physics (GRASP), Utrecht University/Nikhef, Utrecht, Netherlands
- ⁵⁹ Institute of Experimental Physics, Slovak Academy of Sciences, Košice, Slovak Republic
- ⁶⁰ Institute of Physics, Homi Bhabha National Institute, Bhubaneswar, India
- ⁶¹ Institute of Physics of the Czech Academy of Sciences, Prague, Czech Republic
- ⁶² Institute of Space Science (ISS), Bucharest, Romania
- ⁶³ Institut für Kernphysik, Johann Wolfgang Goethe-Universität Frankfurt, Frankfurt, Germany
- ⁶⁴ Instituto de Ciencias Nucleares, Universidad Nacional Autónoma de México, Mexico City, Mexico
- ⁶⁵ Instituto de Física, Universidade Federal do Rio Grande do Sul (UFRGS), Porto Alegre, Brazil
- ⁶⁶ Instituto de Física, Universidad Nacional Autónoma de México, Mexico City, Mexico
- ⁶⁷ iThemba LABS, National Research Foundation, Somerset West, South Africa
- ⁶⁸ Jeonbuk National University, Jeonju, Republic of Korea
- ⁶⁹ Johann-Wolfgang-Goethe Universität Frankfurt Institut für Informatik, Fachbereich Informatik und Mathematik, Frankfurt, Germany
- ⁷⁰ Korea Institute of Science and Technology Information, Daejeon, Republic of Korea
- ⁷¹ KTO Karatay University, Konya, Turkey
- ⁷² Laboratoire de Physique des 2 Infinis, Irène Joliot-Curie, Orsay, France
- ⁷³ Laboratoire de Physique Subatomique et de Cosmologie, Université Grenoble-Alpes, CNRS-IN2P3, Grenoble, France
- ⁷⁴ Lawrence Berkeley National Laboratory, Berkeley, California, United States
- ⁷⁵ Lund University Department of Physics, Division of Particle Physics, Lund, Sweden
- ⁷⁶ Nagasaki Institute of Applied Science, Nagasaki, Japan
- ⁷⁷ Nara Women's University (NWU), Nara, Japan
- ⁷⁸ National and Kapodistrian University of Athens, School of Science, Department of Physics, Athens, Greece
- ⁷⁹ National Centre for Nuclear Research, Warsaw, Poland
- ⁸⁰ National Institute of Science Education and Research, Homi Bhabha National Institute, Jatni, India
- ⁸¹ National Nuclear Research Center, Baku, Azerbaijan
- ⁸² National Research and Innovation Agency - BRIN, Jakarta, Indonesia
- ⁸³ Niels Bohr Institute, University of Copenhagen, Copenhagen, Denmark
- ⁸⁴ Nikhef, National institute for subatomic physics, Amsterdam, Netherlands
- ⁸⁵ Nuclear Physics Group, STFC Daresbury Laboratory, Daresbury, United Kingdom
- ⁸⁶ Nuclear Physics Institute of the Czech Academy of Sciences, Husinec-Řež, Czech Republic
- ⁸⁷ Oak Ridge National Laboratory, Oak Ridge, Tennessee, United States
- ⁸⁸ Ohio State University, Columbus, Ohio, United States
- ⁸⁹ Physics department, Faculty of science, University of Zagreb, Zagreb, Croatia
- ⁹⁰ Physics Department, Panjab University, Chandigarh, India
- ⁹¹ Physics Department, University of Jammu, Jammu, India

- ⁹² Physics Department, University of Rajasthan, Jaipur, India
- ⁹³ Physics Program and International Institute for Sustainability with Knotted Chiral Meta Matter (SKCM2), Hiroshima University, Hiroshima, Japan
- ⁹⁴ Physikalisches Institut, Eberhard-Karls-Universität Tübingen, Tübingen, Germany
- ⁹⁵ Physikalisches Institut, Ruprecht-Karls-Universität Heidelberg, Heidelberg, Germany
- ⁹⁶ Physik Department, Technische Universität München, Munich, Germany
- ⁹⁷ Politecnico di Bari and Sezione INFN, Bari, Italy
- ⁹⁸ Research Division and ExtreMe Matter Institute EMMI, GSI Helmholtzzentrum für Schwerionenforschung GmbH, Darmstadt, Germany
- ⁹⁹ Saha Institute of Nuclear Physics, Homi Bhabha National Institute, Kolkata, India
- ¹⁰⁰ School of Physics and Astronomy, University of Birmingham, Birmingham, United Kingdom
- ¹⁰¹ Sección Física, Departamento de Ciencias, Pontificia Universidad Católica del Perú, Lima, Peru
- ¹⁰² Stefan Meyer Institut für Subatomare Physik (SMI), Vienna, Austria
- ¹⁰³ SUBATECH, IMT Atlantique, Nantes Université, CNRS-IN2P3, Nantes, France
- ¹⁰⁴ Suranaree University of Technology, Nakhon Ratchasima, Thailand
- ¹⁰⁵ Technical University of Košice, Košice, Slovak Republic
- ¹⁰⁶ The Henryk Niewodniczanski Institute of Nuclear Physics, Polish Academy of Sciences, Cracow, Poland
- ¹⁰⁷ The University of Texas at Austin, Austin, Texas, United States
- ¹⁰⁸ Universidad Autónoma de Sinaloa, Culiacán, Mexico
- ¹⁰⁹ Universidade de São Paulo (USP), São Paulo, Brazil
- ¹¹⁰ Universidade Estadual de Campinas (UNICAMP), Campinas, Brazil
- ¹¹¹ Universidade Federal do ABC, Santo Andre, Brazil
- ¹¹² University of Cape Town, Cape Town, South Africa
- ¹¹³ University of Houston, Houston, Texas, United States
- ¹¹⁴ University of Jyväskylä, Jyväskylä, Finland
- ¹¹⁵ University of Kansas, Lawrence, Kansas, United States
- ¹¹⁶ University of Liverpool, Liverpool, United Kingdom
- ¹¹⁷ University of Science and Technology of China, Hefei, China
- ¹¹⁸ University of South-Eastern Norway, Kongsberg, Norway
- ¹¹⁹ University of Tennessee, Knoxville, Tennessee, United States
- ¹²⁰ University of the Witwatersrand, Johannesburg, South Africa
- ¹²¹ University of Tokyo, Tokyo, Japan
- ¹²² University of Tsukuba, Tsukuba, Japan
- ¹²³ University Politehnica of Bucharest, Bucharest, Romania
- ¹²⁴ Université Clermont Auvergne, CNRS/IN2P3, LPC, Clermont-Ferrand, France
- ¹²⁵ Université de Lyon, CNRS/IN2P3, Institut de Physique des 2 Infinis de Lyon, Lyon, France
- ¹²⁶ Université de Strasbourg, CNRS, IPHC UMR 7178, F-67000 Strasbourg, France, Strasbourg, France
- ¹²⁷ Université Paris-Saclay Centre d'Etudes de Saclay (CEA), IRFU, Département de Physique Nucléaire (DPHN), Saclay, France
- ¹²⁸ Università degli Studi di Foggia, Foggia, Italy
- ¹²⁹ Università del Piemonte Orientale, Vercelli, Italy
- ¹³⁰ Università di Brescia, Brescia, Italy
- ¹³¹ Variable Energy Cyclotron Centre, Homi Bhabha National Institute, Kolkata, India
- ¹³² Warsaw University of Technology, Warsaw, Poland
- ¹³³ Wayne State University, Detroit, Michigan, United States
- ¹³⁴ Westfälische Wilhelms-Universität Münster, Institut für Kernphysik, Münster, Germany
- ¹³⁵ Wigner Research Centre for Physics, Budapest, Hungary
- ¹³⁶ Yale University, New Haven, Connecticut, United States
- ¹³⁷ Yonsei University, Seoul, Republic of Korea
- ¹³⁸ Zentrum für Technologie und Transfer (ZTT), Worms, Germany
- ¹³⁹ Affiliated with an institute covered by a cooperation agreement with CERN
- ¹⁴⁰ Affiliated with an international laboratory covered by a cooperation agreement with CERN.